All Actuaries Summit
New age, new actuary

11-13 June 2025, Sydney

Dynamic Financial Analysis (DFA) of General Insurers under Climate Change

Prepared by **Benjamin Avanzi, Yanfeng Li, Greg Taylor, Bernard Wong**

Presented to the Actuaries Institute
2025 All-Actuaries Summit
11-13 June 2025

Actuaries Institute
ABN 69 000 423 656
Level 2, 50 Carrington Street, Sydney NSW 2000
P +61 (0) 2 9239 6100 | actuaries.asn.au

Dynamic Financial Analysis (DFA) of General Insurers under Climate Change

Benjamin Avanzi[a], Yanfeng Li[b,*], Greg Taylor[b], Bernard Wong[b]

[a] *Centre for Actuarial Studies, Department of Economics, University of Melbourne VIC 3010, Australia*
[b] *School of Risk and Actuarial Studies, UNSW Business School, UNSW Sydney NSW 2052, Australia*

Abstract

Climate change is expected to significantly affect the physical, financial, and economic environments over the long term, posing risks to the financial health of general insurers. To navigate these challenges, general insurers need a comprehensive understanding of the impact of climate change. General insurers typically use Dynamic Financial Analysis (DFA) for a comprehensive view of financial impacts, but traditional DFA in academic literature often does not consider the impact of climate change. To address this gap, this study introduces a climate-dependent DFA approach that integrates climate risk into DFA, providing a comprehensive assessment of the long-term impact of climate change on the general insurance industry.

The proposed framework has three key features. First, it captures the long-term impact of climate change on the assets and liabilities of general insurers by considering both physical and economic dimensions across different climate scenarios within an interconnected structure. Second, it addresses the uncertainty of climate change impacts using stochastic simulations within climate scenario analysis that are useful for actuarial applications. Finally, the framework is tailored to the general insurance sector by addressing its unique characteristics.

To demonstrate the practical application of our model, we conduct an extensive empirical study using Australian data to assess the long-term financial impact of climate change on the general insurance market under various climate scenarios, which is enabled by our modelling design. The results show that the interaction between economic growth and physical risk plays a key role in shaping general insurers' risk-return profiles. It should be noted that our analysis is based on the climate scenarios as defined because our focus is on their implications for general insurers. The limitations of the scenarios themselves are left for future research.

Keywords: Climate change, Dynamic Financial Analysis, General insurance
JEL Codes: C51, C53, G22
MSC classes: 91G70, 91G60, 62P05, 91B30

* Corresponding author.

Email addresses: b.avanzi@unimelb.edu.au (Benjamin Avanzi), yanfeng.li@student.unsw.edu.au (Yanfeng Li), gregory.taylor@unsw.edu.au (Greg Taylor), bernard.wong@unsw.edu.au (Bernard Wong)

1 Introduction

1.1 Background

Climate change poses a multifaceted and profound impact on the financial performance and position of general insurers. On the liabilities side, shifting weather patterns are likely to alter the frequency and severity of future claims (see, e.g., Haug et al., 2011; Lyubchich et al., 2019), which could lead to increased claims costs and adversely affect underwriting profitability. On the assets side, climate change-induced fluctuations in temperature, shifting patterns of natural disasters, and evolving socio-economic conditions may significantly influence key macroeconomic variables. These include inflation rates (see, e.g., Parker, 2018; Economides and Xepapadeas, 2018; Kotz et al., 2024), interest rates (see, e.g., Bylund and Jonsson, 2020; Mongelli et al., 2022), and equity returns (see, e.g., Karydas and Xepapadeas, 2022; Venturini, 2022; Barnett, 2023), thereby impacting the investment performance of general insurers. Ultimately, the combined effects of climate change on both assets and liabilities will cascade into insurers' capital positions, potentially affecting the financial health and stability of the broader general insurance market.

To navigate these challenges, a comprehensive understanding of climate change's impact on general insurers is essential. This need is increasingly recognised by regulators, as evidenced by the growing number of climate-related disclosure requirements, such as IFRS S2 (IFRS, 2023) and its Australian equivalent, AASB S2 (AASB, 2023). Efforts have been made to incorporate climate change impacts into the modelling of insurance liabilities and assets, yet a comprehensive approach remains limited. On the liabilities side, various studies have examined climate change effects on hazards such as floods (see, e.g., Seneviratne et al., 2021), bushfires (see, e.g., Quilcaille et al., 2022), and tropical cyclones and storms (see, e.g., Jagger et al., 2008, 2011; Meiler et al., 2022), generally indicating that rising temperatures exacerbate the frequency and severity of most hazard events (IPCC, 2021a). Additionally, the impact of climate change on non-catastrophe, weather-related claims frequency and severity have also been investigated in literature(see, e.g., Haug et al., 2011; Lyubchich et al., 2017). On the assets side, climate change impacts on interest rates, inflation rates, and equity returns have been explored both theoretically using General Equilibrium Models (Economides and Xepapadeas, 2018; Karydas and Xepapadeas, 2022; Barnett, 2023) and empirically using multiple regression (see, e.g., Parker, 2018) and Factor Models (see, e.g., Venturini, 2022). However, most studies typically focus on individual financial items, with comprehensive analyses examining the interconnected financial impacts of climate change on general insurers across both assets and liabilities remaining limited in the current literature.

A widely used tool in the general insurance industry for informing strategic decisions is Dynamic Financial Analysis (DFA). DFA offers a comprehensive perspective on the financial impacts that affect general insurers (Coutts and Devitt, 1989; Paulson and Dixit, 1989; Kaufmann et al., 2001; Eling and Toplek, 2009). It encompasses a suite of methods designed to project and analyse the future financial position of insurers under various scenarios. Typical applications of DFA include economic capital modelling, solvency monitoring, and strategy testing. Additionally, it functions as a model office, enabling management to evaluate current strategies in a theoretical environment under different scenarios, thereby helping to avoid costly real-world errors (Kaufmann et al., 2001; Eling and Parnitzke, 2007). It can also be employed to analyse market behaviors within the general insurance sector (see, e.g., Taylor, 2008). However, existing DFA frameworks in literature (see, e.g., Kaufmann et al., 2001; D'Arcy and Gorvett, 2004; Consigli et al., 2018) do not explicitly incorporate climatic factors, which limits their effectiveness in addressing the financial implications of climate change. To address this gap, we propose a comprehensive yet tractable "climate-dependent DFA" framework for examining the multifaceted impacts of climate change on the general insurance market, as detailed in the following section.

1.2 Statement of contributions

In this paper, we extend the traditional DFA framework by integrating climate change considerations to provide a comprehensive assessment of climate impacts on general insurance markets. This framework can serve as an initial step in guiding decision-making for both insurers and regulators facing climate-related challenges. Specifically, we propose the *"climate-dependent DFA"* framework, designed to address key attributes of climate change impacts within the general insurance context:

- *Comprehensive nature of climate impacts*: Extensive studies have shown that climate change can influence both insurance claims and investment returns as discussed in the previous section, affecting the assets and liabilities of general insurers. However, most of these studies consider these impacts in isolation. Given the interdependencies between assets and liabilities, such an isolated approach may underestimate the overall financial impact of climate change on general insurers. Furthermore, widely used climate scenarios–such as the Shared Socioeconomic Pathways (SSP) developed by the IPCC (O Neill et al., 2017)–combine both physical and economic narratives, necessitating a comprehensive modelling framework to fully account for these interconnected aspects.

  In this paper, we introduce a *comprehensive* yet *tractable* "climate-dependent DFA" framework to support decision-making for general insurers and regulators confronting climate-related challenges. By leveraging the interconnected structure of the traditional DFA framework, our approach integrates the physical and economic aspects of each climate scenario, ensuring that both asset– and liability– related impacts are captured. This is particularly advantageous for decision areas influenced by both assets and liabilities, such as economic capital modelling, capital planning, and solvency monitoring. Meanwhile, we base our framework on tractable models to maintain transparency and interpretability, which are critical elements in effective management decisions (Eling and Parnitzke, 2007), and to avoid obscuring key insights with unnecessary complexity.

- *Long-term nature of climate change*: Climate change is inherently long-term, and it is usually challenging to distinguish the effects of global warming from internal variability over short horizons; indeed, internal variability ranges from inter-annual (e.g., El Niño–Southern Oscillation) to inter-decadal (e.g., Atlantic Multi-decadal Variability) (IPCC, 2021a). In addition, new regulations – such as IFRS S2 (IFRS, 2023) and AASB S2 (AASB, 2023) – require insurers to disclose the long-term financial impacts of climate change. A longer-term perspective is also essential for decisions by insurers and policymakers that extend across multiple years, including relocation planning (typically 8 to 40 years (Bower and Weerasinghe, 2021)) and reinsurance planning (influenced by cycles of about 9 to 11 years (Meier and Outreville, 2006, 2010)).

  An initial attempt to measure climate change effects on both assets and liabilities of general insurers simultaneously is presented in Gatzert and Özdil (2024), albeit limited to a one-year horizon. Our proposed framework utilizes a multi-year perspective within a DFA structure to assess the cumulative effects of climate change on general insurers, effectively capturing its long-term nature as previously discussed.

- *Uncertainty in climate change impacts*: The path of future climate is heavily influenced by the evolution of human society; consequently, scenario analysis is frequently employed in climate change assessments to capture this uncertainty (O Neill et al., 2017). Although traditional DFA models attempt to generate a wide range of potential outcomes using stochastic simulations (Kaufmann et al., 2001), they do not incorporate key qualitative societal factors – such as environmental awareness, education quality, and political stability – that are critical for projecting future climate developments (O Neill et al., 2017). Moreover, many commonly used climate scenarios are deterministic in nature (O Neill et al., 2017; Bertram et al., 2020), whereas general insurance actuarial applications, such as economic capital modelling, require both central and distributional forecasts.

  In this paper, we embed stochastic simulations within climate scenario analysis to address these gaps. Our proposed framework accounts for the uncertainty arising from future societal developments, as well as the inherent randomness in natural and financial systems. By allowing users to simulate a distribution of financial outcomes across different climate pathways, the framework supports the assessment of future financial performance under both expected returns and risks, which are key considerations for insurers, actuaries, and regulators. Note that our analysis seek to incorporate the economic and environmental assumptions of each climate scenario to assess their implications for general insurers, while evaluating the validity of those assumptions is beyond the scope of this paper.

Finally, as illustrated above, our proposed framework is specifically designed for the general insurance sector by incorporating its unique features: it accounts for the interdependence between assets and liabilities through its interconnected structure and captures the high variability of liability cash flows using the DFA's stochastic simulations. In addition, we include catastrophe reinsurance programs and consider the effects of reinsurance cycles, which is another important factor influencing insurers' profitability and solvency (see, e.g., Meier and Outreville, 2006).

To illustrate its practical application, we implement the proposed framework in the Australian context. Australia's geography and climate make it especially prone to extreme weather events such as bushfires, floods, and tropical cyclones. Climate change will intensify many of these hazards particularly in high-emission scenarios (IPCC, 2021b). This may place increasing pressure on insurers' capacity to underwrite coverage and maintain solvency. To capture these evolving conditions, we calibrate the framework's parameters using real Australian data on insurance losses, macroeconomic indicators, and financial markets, providing realistic insights into the long-term climate impacts on the Australian general insurance market.

1.3 Scope of the paper

The primary objective of this paper is to provide insights into industry-wide trends over a long-term horizon under the impact of climate change, rather than to inform short-term, insurer-specific decision-making. To achieve this, a macro-level modelling framework is adopted, which focuses on national-level projections of climate change impacts on the general insurance industry. Accordingly, both the subnational-level modelling of hazards and socio-economic variables, and the use of such outputs to inform granular decision-making, such as portfolio steering or individual risk pricing, are considered outside the scope of this study. The aim is to establish a generalised and scalable framework, rather than one tailored to any specific insurer. Nevertheless, individual insurers may build upon this foundation by incorporating greater model granularity and integrating tools such as proprietary catastrophe models (Mitchell-Wallace et al., 2017) to develop customised models aligned with their own risk profiles and exposures.

It is also worth mentioning that this paper presents an illustrative example of climate change impacts on the general insurance market, aimed at demonstrating the application of the proposed framework. It should not be interpreted as a complete predictive analysis for any specific country (e.g., Australia). The scope of this study is to illustrate what is possible when integrating climate considerations into DFA, and to highlight the high-level insights that can be drawn regarding the potential impacts of climate change on the general insurance sector.

Finally, this study aims to provide a baseline model to assess the financial impact of climate change on the general insurance market, excluding the influence of short-term policy changes or regulatory interventions. However, relevant stakeholders can explore the effects of various government or regulatory actions by applying modifications to the proposed model and comparing the outcomes against the baseline.

1.4 Outline of the paper

In Section 2, we introduce the modelling framework for the proposed climate-dependent DFA. Section 2.1 then provides an overview of the structure of this framework. The design of its component modules is discussed from Section 2.2 through Section 2.4.

In Section 3, we present and analyse the numerical simulation outcomes – calibrated using Australian data – generated by the proposed framework. Section 4 concludes the paper, and Section 5 discusses the limitations and potential directions for future research.

2 Model framework

In this section, we begin by outlining the scenarios employed with their limitations acknowledged and providing an overview of our proposed framework's structure. We then detail the design of the component modules within the climate-dependent DFA framework, which collectively enable users to capture the comprehensive impacts of climate change on general insurers. Specifically, Section 2.2 introduces the climate and hazards modules, which simulate both climate variables and the frequency and severity of natural catastrophes over the projection horizon. Subsequently, Sections 2.3 and 2.4 describe the assets and liabilities modules, respectively, which project future investment returns and underwriting results under each climate scenario, based on outputs from the climate and hazards modules. Finally, Section 2.5 introduces the surplus module, which combines outputs from both the assets and liabilities modules, and presents key measures of general insurance financial performance.

2.1 Model overview

The proposed climate-dependent DFA framework is illustrated in Figure 2.1. A key input to this framework is the set of climate scenarios, for which we adopt the Shared Socioeconomic Pathways (SSPs). These SSPs form a widely adopted framework in climate research and they are central to the IPCC's climate risk assessments (O Neill et al., 2017). Each SSP scenario is associated with a narrative, from which the economic growth rate at the technological frontier is derived (Dellink et al., 2017a). Starting from historical values, country-specific GDP projections are generated under the assumption that individual economies gradually converge toward this frontier. The convergence speed is determined by the degree of trade openness, as inferred from the scenario narratives (Dellink et al., 2017a). The emissions pathways consistent with the economic and environmental assumptions underlying each scenario are then used as inputs to climate models to produce projections of future climate at a much finer spatial resolution, typically at the level of gridded cells (Eyring et al., 2016).

The narratives of the selected representative climate scenarios are outlined below (O Neill et al., 2017):

- SSP 2.6 ("Sustainability"): Envisions a world characterised by progressive economic development and improving environmental conditions. The combination of low physical risk and sustainable economic growth results in low challenges for both mitigation and adaptation.
- SSP 4.5 ("Middle of the Road"): Represents a development pathway aligned with typical historical trends observed over the past century, leading to moderate mitigation and adaptation challenges.
- SSP 7.0 ("Regional rivalry"): Describes a world characterised by slowing economic growth and environmental degradation due to regional rivalries. Here, the combination of weak economic growth and elevated physical risk gives rise to high mitigation and adaptation challenges.
- SSP 8.5 ("Taking the highway"): Describes a world with rapid economic growth driven by competitive markets and innovation. Heavy reliance on fossil fuels, however, contributes to high physical risk and consequently high mitigation challenges, though strong economic growth leads to relatively low adaptation challenges.

A distinct feature of our framework is its interconnected design, allowing it to capture interactions among the various financial dimensions of general insurers. Beginning at the top of the diagram, we use the future climate and socioeconomic projections from each SSP scenario as inputs for modelling other variables within the DFA framework, following the cascading structure illustrated in the figure.

The projections of climate variables underlying each SSP scenario are used to estimate the frequency and severity of major natural hazard events in Australia, thereby generating the market-level catastrophe insurance losses. On the liabilities side, these catastrophe loss estimates translate into claims liabilities for general insurers, taking into account their reinsurance structures and market shares. On the assets side, socioeconomic projections under each SSP scenario, along with climate damage estimates from the hazards module, inform the simulation of investment returns. Finally, combining the resulting asset and liability forecasts allows us to derive the surplus of general insurers, representing an overall measure of market-wide financial performance.

In essence, the interconnected nature of our proposed framework captures both direct and indirect climate change impacts. By recognising dependencies among various financial components, it offers a comprehensive view of climate change's impact on the general insurance sector.

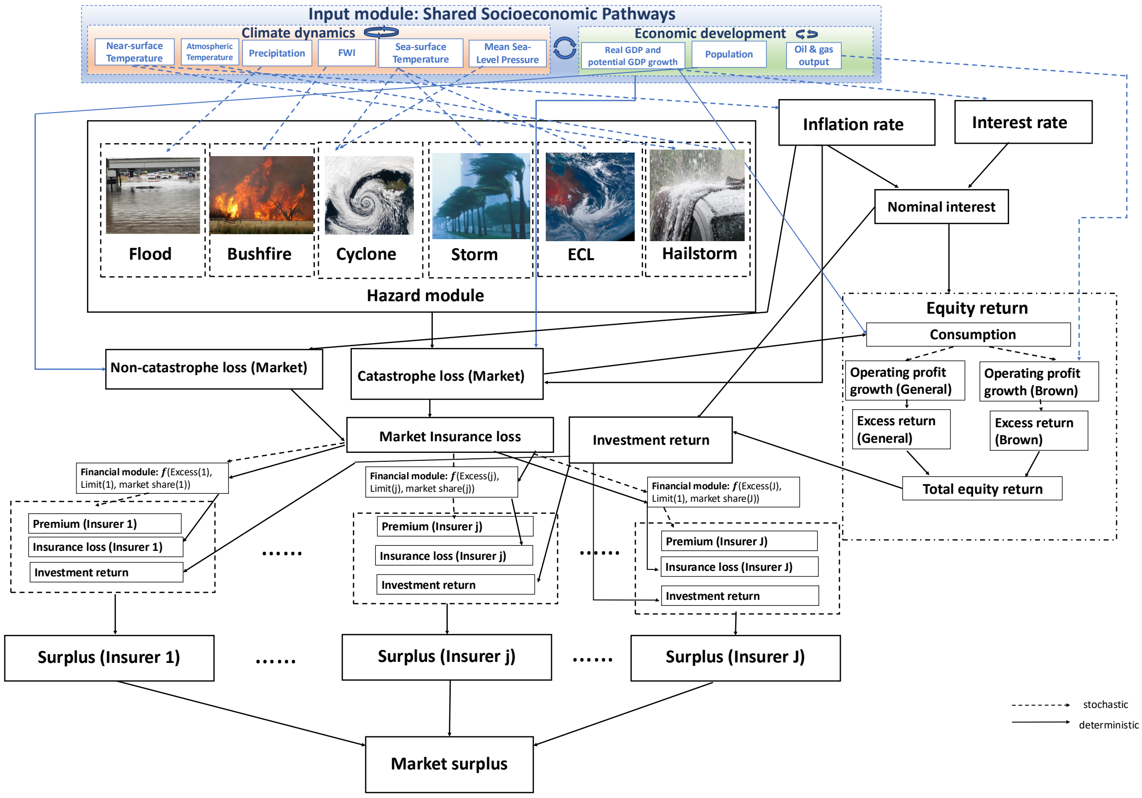

Figure 2.1: Modelling framework of climate-dependent DFA

Remark 2.1. *Note that caution is warranted when interpreting the results derived from these scenarios, given the limitations of their underlying assumptions, particularly under high-emission pathways such as SSP 8.5. This scenario assumes continued economic growth in a high-temperature environment without accounting for climate tipping points, i.e., significant and potentially irreversible changes triggered by global warming that could cause economic collapse (Keen et al., 2021). However, the timing of such tipping points remains debated: while some climate–economy models assume they will not occur within the next 300 years (e.g., Nordhaus, 2013), other studies suggest they could be triggered before 2100 (e.g., Lenton et al., 2008).*

Another potential limitation of the economic growth assumptions in the SSP scenarios, as well as in other climate scenarios such as DICE (Nordhaus, 1992, 2018; Barrage and Nordhaus, 2024), is that labour productivity is treated as exogenous, without accounting for the potential adverse effects of climate change (Keen et al., 2021). Yet, research has shown that rising temperatures above human comfort levels can negatively impact human health (Mora et al., 2017) and reduce labour productivity (Heal and Park, 2016). However, it is also worth noting that the SSP 8.5 narrative assumes "strong investments in health, education, and institutions to enhance human and social capital," alongside "highly engineered infrastructure" (O Neill et al., 2017), which could help mitigate climate-related productivity losses. Nonetheless, the extent of such mitigation remains uncertain. The validation and potential refinement of these scenario assumptions are beyond the scope of this paper and are left for future research.

Remark 2.2. *This study focuses on the direct financial impacts of climate change on general insurers, as outlined in the modelling framework presented in Figure 2.1. While indirect effects, such as* *shifts in customer preference toward "greener" insurers or the potential rise in liability risks (e.g., lawsuits against commercial policyholders for environmental damage (Alien, 2003; Bullock, 2022)), are not included here, these are important areas for future research. As quantitative methodologies for assessing such risks continue to evolve, their integration into DFA frameworks may become more feasible.*

2.2 Climate and hazards

2.2.1. Climate module

The raw forecasts of climate variables (e.g., temperature, precipitation, and sea-level pressure) are derived from outputs of the Coupled Model Intercomparison Project Phase 6 (CMIP6). The findings based on the CMIP6 models play a crucial role in informing the IPCC Sixth Assessment Report (IPCC, 2021a). CMIP6 comprises a set of global climate model experiments that simulate historical, present and future climate conditions under IPCC's SSP scenarios (Eyring et al., 2016). CMIP6 model outputs are typically provided as gridded datasets, representing climate variables across latitude–longitude grids over time, with spatial resolutions ranging from 1° to 2.5°. These outputs are aggregated by averaging across grid cells within defined regions, with the selection of regions for each hazard type discussed in detail in Section 2.2.2.

One limitation of the raw outputs from CMIP6 models is that they are deterministic in nature. As highlighted in Section 1.2, it is essential for actuarial applications, especially capital modelling, to incorporate the stochastic variability (i.e., aleatoric uncertainty) of climate forecasts. Additionally, model outputs can exhibit biases relative to observations (often due to resolution discrepancies) (Haug et al., 2011; Maraun, 2013). Furthermore, uncertainties can also arise from limitations in the climate models used (i.e., model uncertainty) (Liu and Raftery, 2021).

To address these biases and both aleatoric and model uncertainty, we adopt the following procedure for simulating future climate variables (see Figure 2.2), building on the approach of Liu and Raftery (2021):

1. *Model uncertainty:* We use an ensemble of CMIP6 models to capture differences among future climate forecasts (Liu and Raftery, 2021). This ensemble approach acknowledges that distinct models can yield varying projections.
2. *Bias correction:* For each ensemble member, we correct bias by comparing model backcasts to historical observations via the quantile mapping method, a simple but effective technique frequently used in the literature (Haug et al., 2011; Maraun, 2013; Sanabria et al., 2022). Specifically, we estimate
$$\hat{\theta}_q \;=\; \hat{\beta}_0^{(m)} \;+\; \hat{\beta}_1^{(m)}\,\hat{\theta}_q^{(m)}, \tag{2.1}$$
where θ_q and $\hat{\theta}_q^{(m)}$ are the q^{th} quantiles of the historical observations and model m backcasts, respectively, over the same reference period.
3. *Aleatoric uncertainty:* To incorporate inherent randomness, we collect residuals $z_t^{(m)} = \theta_t - \hat{\theta}_t^{(m),*}$ by comparing the bias-corrected model backcasts $\hat{\theta}_t^{(m),*}$ with actual historical data θ_t. We then calibrate a Normal distribution on the residuals (i.e., $z_t^{(m)} \sim \mathrm{N}(0, \sigma^2_{(m)})$). Although simplistic, this assumption is supported by normality tests (e.g., Shapiro–Wilk (Yazici and Yolacan, 2007)) for most ensemble members.
4. *Future projections and simulations:* For each simulation path in the future projection period, we randomly select a CMIP6 model m to generate a deterministic forecast $\hat{\theta}_t^{(m)}$. We apply

the bias correction as $\hat{\theta}_t^{(m),*} = \hat{\beta}_0^{(m)} + \hat{\beta}_1^{(m)}\,\hat{\theta}_t^{(m)}$, and then draw one trajectory of residuals $\tilde{z}_t^{(m)}$ to account for aleatoric uncertainty. The final simulated climate variable is thus:

$$\tilde{\theta}_t = \hat{\theta}_t^{(m),*} + \tilde{z}_t^{(m)}. \tag{2.2}$$

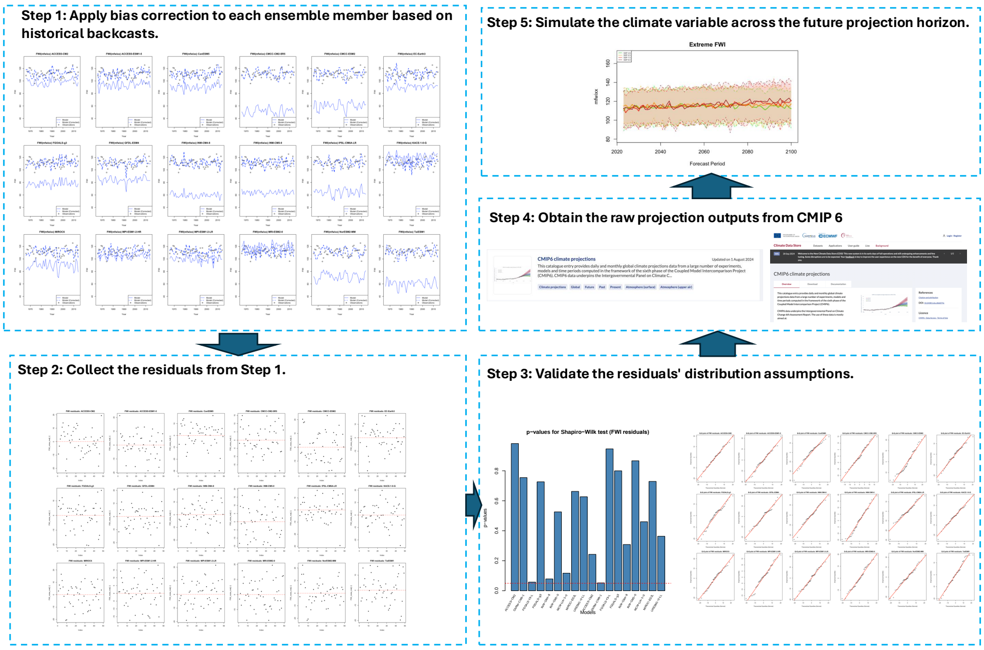

Figure 2.2: An illustrative diagram of climate variable simulations

2.2.2. Hazards module

Based on the projected climate variables from the previous module, this section forecasts the frequency and severity of natural hazards. This constitutes a critical component of the DFA model, as the resulting hazard forecasts will be employed to model the general insurance assets and liabilities in subsequent sections. Numerous approaches exist for hazard modelling in the literature; however, as discussed in Section 1.2, balancing model interpretability and comprehensiveness is essential.

At one extreme, traditional Collective Risk Models (CRMs) (Klugman et al., 2012) offer a simplistic, intuitive means of modelling aggregate insurance losses, and it is also often used in traditional DFA applications (Kaufmann et al., 2001). Yet, their static assumption regarding insurance loss distributions neglects the dynamics introduced by climate change. At the other extreme, CAT models are sophisticated models that are usually capable of capturing the complex environmental process affected by climate change to generate hazard events based on advanced physical and mathematical models (Mitchell-Wallace et al., 2017). However, these proprietary models usually have complex structures with modelling details usually not accessible by general insurers, making them less comprehensible for insurers (Weinkle and Pielke Jr, 2017), leading to challenges in interpretability.

In light of the above considerations, we have opted for the weather-dependent CRMs (Haug et al., 2011) for modelling insurance losses. These models combine the high interpretability of traditional CRMs with the capability to incorporate climate effects by integrating meteorological variables in the modelling of insurance loss frequency and severity. In essence, the aggregate catastrophe loss ($\tilde{X}_t$) is modelled as:

$$\tilde{X}_t = \sum_{i=1}^{I} \sum_{m=1}^{M_t^{(i)}} \tilde{X}_t^{(i),m}, \tag{2.3}$$

where $M_t^{(i)}$ is the number of event of hazard type i in year t, and $\tilde{X}_t^{(i),m}$ is the insurance loss associated with the m^{th} event of hazard type i in year t. We further assume:

$$M_t^{(i)} \sim \text{Poi}(\lambda(\mathbf{\Theta_t^{(i)}})); \quad X_t^{(i),m} \sim \text{LN}(\mu(\mathbf{\Theta_t^{(i)}}), \sigma^2), \tag{2.4}$$

where $\mathbf{\Theta_t^{(i)}}$ is a set of weather covariates for hazard type i, and $X_t^{(i),m}$ is the normalised catastrophe loss adjusted for both inflation and wealth exposure [1]. The Poisson distribution aligns with common practice in modelling the frequency of hazard events (see, e.g., Jagger et al., 2008, 2011). Similarly, Log-Normal distribution is frequently used for modelling catastrophe losses due to its heavy-tailed nature (Kaufmann et al., 2001; McNeil et al., 2015), and it is also selected from a class of heavy-tailed candidates based on our data (see Appendix C.1).

We further specify:

$$\log(\lambda^{(i)}) = \boldsymbol{\beta}'_{\mathbf{(i)}} \mathbf{\Theta_t^{(i)}}; \quad \mu^{(i)} = \boldsymbol{\alpha}'_{\mathbf{(i)}} \mathbf{\Theta_t^{(i)}}, \tag{2.5}$$

where the set of coefficients $\boldsymbol{\beta}_{\mathbf{(i)}}$ and $\boldsymbol{\alpha}_{\mathbf{(i)}}$ are estimated via regression.

We select the weather covariates based on the physical mechanisms driving each hazard type i and validate them statistically. Here, we focus on major Australian hazards: flood, bushfire, tropical cyclones, storms, hailstorm, and East Coast Lows (IPCC, 2021b). Below, we outline the candidate weather covariates for each hazard type, drawn from relevant literature on the associated physical processes.

Bushfire

Bushfire risk depends on temperature, relative humidity, drought conditions, and wind speed (Sharples et al., 2016; Dowdy, 2018; Quilcaille et al., 2022). Generally, fire danger increases with higher temperatures, lower humidity, stronger winds, and more severe drought. The Fire Weather Index (FWI), derived from these factors, is commonly used to assess bushfire risk (Dowdy, 2018; Quilcaille et al., 2022). In particular, bushfire occurrence responds most strongly to extremes of the FWI rather than average conditions (Quilcaille et al., 2022). Hence, we choose:

$$\mathbf{\Theta_t^{(\text{BF})}} = \{\text{fwixx}_t, \text{fwixd}_t\},$$

where fwixx_t is the annual maxima of fire weather index, and fwixd_t is the number of days with extreme fire weather, which are two crucial statistics capturing FWI extremes (Quilcaille et al., 2022). The FWI data is subsequently averaged over the land surface area of Australia to derive a national-level indicator.

Flood

Precipitation, particularly extreme precipitation, is a key driver of pluvial and river floods (Kodra et al., 2020; IPCC, 2021a). Accordingly, we choose:

$$\mathbf{\Theta}_{\mathbf{t}}^{(\mathrm{FL})} = \{R_t^{\mathrm{x5}}, R_t^{\mathrm{x1}}, R_t\},$$

where R_t represents the annual total precipitation, R_t^{x1} is the largest one-day precipitation (usually denoted as `rx1day`), and R_t^{x5} is the largest five-day cumulative precipitation (usually denoted as `rx5day`). Both R_t^{x1} and R_t^{x5} are commonly used as proxies for extreme precipitation in the IPCC report (IPCC, 2021a). Similarly, the precipitation data is then averaged across the Australian land surface area.

Tropical Cyclone and storms

The critical climate drivers for the formation and intensity of cyclones include sea surface temperature (SST) and sea level pressure (Meiler et al., 2022; IPCC, 2021a). Warm ocean water is an essential condition for storm formation; additionally, low sea level pressure contributes to storm development by causing warm, moist air to rise (Bureau of Meteorology). Therefore, storms typically form under conditions of high sea surface temperature and low sea level pressure. When the wind speed exceeds 119 km/h, the storm is classified as a cyclone (Bureau of Meteorology).

To capture the influence of sea surface temperature and sea level pressure on tropical cyclones and storms, we choose:

$$\mathbf{\Theta}_{\mathbf{m}}^{(\mathrm{TC})} = \{\overline{\mathrm{SST}}_m, \overline{\mathrm{MSLP}}_m\},$$

where $\overline{\mathrm{SST}}_m$ is the monthly average sea surface temperature over the Australian Tropical Cyclone Basin [2], and $\overline{\mathrm{MSLP}}_m$ is the monthly average mean sea level pressure over the same region. The use of monthly averages for sea surface temperature and mean sea level pressure is also consistent with common practices in the literature, such as in the CAT model STORM (Bloemendaal et al., 2020).

Hailstorm

Atmospheric and near-surface temperatures are key drivers of hailstorm formation and intensity (Raupach et al., 2021). Rising near-surface temperatures increase low-level moisture and convective instability, potentially boosting hail frequency (Allen et al., 2014; Raupach et al., 2021). Higher atmospheric temperatures contribute to greater water vapor, intensifying hailstorms, but also raise the melting level, which can reduce hail frequency by melting smaller hailstones (Raupach et al., 2021). Thus, the overall impact varies locally, with projections indicating increased hail frequency in Australia (Leslie et al., 2008; Allen et al., 2014; Raupach et al., 2021).

Accordingly, we choose:

$$\mathbf{\Theta}_{m}^{(\mathrm{H})} = \{\bar{T}_m^{\mathrm{NS}}, \bar{T}_m^{\mathrm{MT}}\},$$

where $\bar{T}_m^{\mathrm{NS}}$ is the monthly average near-surface temperature, and $\bar{T}_m^{\mathrm{MT}}$ is the monthly average mid-tropospheric temperature.

East Coast Lows

An East Coast Low (ECL) is a type of mid-latitude cyclone that forms near the east coast of Australia, commonly referred to as the ECL identification region (Pepler et al., 2016a,b; Speer et al., 2021). However, the formation mechanisms of ECLs differ from those of tropical cyclones. While tropical cyclones develop over warm ocean waters, ECL formation is primarily driven by sea-surface temperature gradients (Pepler et al., 2016a).

Based on the above mechanism, we choose:

$$\boldsymbol{\Theta}_{\mathbf{m}}^{(\mathrm{ECL})} = \{\Delta\overline{\mathrm{SST}}_m, \overline{\mathrm{SST}}_m\},$$

where $\Delta\overline{\mathrm{SST}}_m$ represents the SST gradient near the east coast of Australia, defined as the average difference between $\overline{\mathrm{SST}}_m$ in the region spanning $24°$–$41°$S and $148°$–$155°$E, and $\overline{\mathrm{SST}}_m$ in the corresponding region spanning $24°$–$41°$S and $160°$–$165°$E (Pepler et al., 2016a).

Remark 2.3. *The hazard loss modelling in this study does not explicitly incorporate potential government interventions, such as the introduction of the Australian Cyclone Reinsurance Pool in 2022 (Jarzabkowski et al., 2022). As discussed in Section 1.3, the primary aim of this work is to develop a general framework, rather than a complete predictive analysis for any specific country. As a baseline model, it can serve as a foundation for future studies to explore the potential impacts of various policy interventions.*

Remark 2.4. *Our forecasts of hazard-related losses are derived from historically calibrated relationships between climate variables and observed insurance losses. However, these relationships may change, especially under the impact of tipping points (Neal et al., 2025). Future research could improve hazard modelling by incorporating tipping point effects and conducting sensitivity analyses to account for the high degree of uncertainty in their timing, triggers, and impact magnitude (Lenton et al., 2008; Nordhaus, 2013).*

2.3 Assets and macro-economic variables

2.3.1. Inflation rates

General inflation rates can influence both the liabilities and assets of general insurers by affecting claims inflation and nominal interest rates (Kaufmann et al., 2001). Baseline inflation rates are modelled following the common approaches in literature by using the mean-reverting AR(1) process (see, e.g., Chen et al., 2021; Bégin, 2022):

$$i_t = \mu_i + a_i(i_{t-1} - \mu_i) + \sigma_i \epsilon_{i,t}, \tag{2.6}$$

where i_t denotes the inflation rate at time t, μ_i is the long-run mean inflation, a_i is the autoregressive parameter, σ_i is the volatility, and $\epsilon_{i,t}$ represents a standard error term.

Studies have shown that historical fluctuations in weather conditions – such as temperature shocks and increased temperature variability – can exert inflationary pressures on food, energy, and service prices (Faccia et al., 2021; Mukherjee and Ouattara, 2021; Ciccarelli et al., 2023). This inflationary effect ultimately contributes to general inflation. Since climate change is expected to exacerbate weather fluctuations, it is crucial to account for its impact in modelling inflation rates (Kotz et al., 2024). To incorporate the influence of climate on inflation, we apply a climate overlay to the baseline inflation rates, following the methodology proposed by Kotz et al. (2024). To the best of our knowledge, the study by Kotz et al. (2024) is the first to quantitatively assess and project the effects of future climate change on both food and general inflation. Specifically, the climate-adjusted inflation rate is given by:

$$i_t^{\text{Clim}} = i_t + i_t^{\text{Clim-Impact}}, \tag{2.7}$$

where $i_t^{\text{Clim-Impact}}$ captures the additional inflationary effects from climate change. Following the approach in Kotz et al. (2024), the monthly climate impact on inflation is modelled as:

$$i_m^{\text{Clim-Impact}} = \sum_{L=1}^{11} (\alpha_{1+L} \Delta \bar{T}_{m-L}^{\text{NS}} + \beta_{1+L} \bar{T}_{m-L}^{\text{NS}} \cdot \Delta \bar{T}_{m-L}^{\text{NS}}), \tag{2.8}$$

where $\bar{T}_m^{\text{NS}}$ denotes the monthly average near-surface temperature over Australia and $\Delta \bar{T}_m^{\text{NS}}$ represents the deviation of future monthly averages from the 1990–2021 baseline. This formulation assumes a one-year lag effect. The term β_{1+L}, $\bar{T}_{m-L}^{\text{NS}} \cdot \Delta \bar{T}_{m-L}^{\text{NS}}$ is introduced to capture the interaction effect whereby higher temperatures during hotter months lead to larger inflationary impacts (Faccia et al., 2021; Kotz et al., 2024). For future projections, the monthly average near-surface temperature will be sourced from the outputs of the climate module described in Section 2.2.1. The annual climate impact on inflation rates for year t is then obtained by summing the monthly impacts (Kotz et al., 2024): $i_t^{\text{Clim-Impact}} = \sum_{m \in t} i_m^{\text{Clim-Impact}}$.

2.3.2. Risk-free interest rates

Drawing inspiration from Laubach and Williams (2003) and Holston et al. (2017), we model the real risk-free short-term interest rate as:

$$r_t = \beta_0 + \beta_1 g_t + z_t, \tag{2.9}$$

which is closely related to the Ramsey's equation (Ramsey, 1928), given by $r^* = \rho + \gamma g$, where g denotes the growth rate of potential output, ρ represents the rate of time preference, and r^* denotes the natural rate of interest. A positive relationship between r^* and g is expected, as higher potential growth enhances future income prospects, reducing households' incentives to save today and thereby placing upward pressure on natural rate of interest (Mongelli et al., 2022).

In our model, g_t denotes the growth rate of potential real GDP. For calibration, these growth rates will be obtained from the World Bank Potential Growth Database (Kilic Celik et al., 2023). For future projections, g_t will be derived from the GDP forecasts under each SSP scenario provided in the SSP database (Riahi et al., 2017). The residual term z_t is assumed to follow an AR(1) process:

$$z_t = \mu_r + \phi_r(z_{t-1} - \mu_r) + \epsilon_r(t), \tag{2.10}$$

which captures residual factors not explained by the growth rate. The nominal risk-free rate is then derived by incorporating inflationary effects using Fisher's equation: $\tilde{r}_t = r_t + i_t^{\text{Clim}}$.

In summary, the key inputs for this model are the real GDP growth rate g_t and the climate-adjusted inflation rate i_t^{Clim} (as output from the inflation model; see Section 2.3.1). These inputs yield the nominal risk-free rate, $\tilde{r}_t$, as the final output.

Remark 2.5. *Choice of g_t: To mitigate the potential endogeneity issue, here g_t is chosen as the growth rate of potential (full-capacity) GDP in the historical calibration; for future forecasts, g_t will be derived from the potential real GDP forecasts underlying each SSP scenario (Dellink et al., 2017b). Therefore, the impact of monetary policy (through manipulation of i_t) on g_t is limited, as it mainly affects short-term output gaps.*

2.3.3. Equity module

We begin by considering the benchmark equity return model proposed by Ahlgrim et al. (2005), which is given by:

$$r_t^{(S)} = \tilde{r}(t) + x_t, \tag{2.11}$$

where $\tilde{r}(t)$ is the nominal risk-free rates, and x_t is the excess equity return.

Under traditional DFA or ESG frameworks (see, e.g., Wilkie, 1995; Ahlgrim et al., 2005; Chen et al., 2021; Bégin, 2022), excess equity returns are often modelled as independent stochastic processes, which is a self-contained approach that can enhance reliability in light of the considerable uncertainty surrounding exogenous variables over long-term horizons (Wilkie, 1995). However, relying solely on historical data limits the capacity to capture the forward-looking climate impacts and the evolving socio-economic conditions under different scenarios.

By contrast, factor models leverage a wide range of climate proxies – often at a granular level – to assess their influence on equity returns (see, e.g., Bansal et al., 2019; Hong et al., 2019; Görgen et al., 2020; Venturini, 2022). While these models are effective for empirical, in-sample analyses of individual or portfolio assets, their extensive data requirements and focus on asset-specific rather than market-level returns pose challenges for long-term projections, whereas ESG or DFA typically focuses on market-level returns.

To strike a balance between these two approaches, we propose a partial self-contained framework that incorporates forward-looking climate considerations without relying on overly granular external data. Inspired by the climate-economic literature (see, e.g., Karydas and Xepapadeas, 2022; Barnett, 2023), our method channels climate's influence on equity returns through climate-damaged consumption. In our historical calibration, excess total equity returns are modelled as a function of corporate earnings growth, $\Delta \mathrm{OP}_t$, which is itself modelled as a function of consumption growth, ΔC_t. Specifically, we have:

$$x_t = \beta_0 + \beta_1 \Delta \mathrm{OP}_t + \epsilon_t^{\mathrm{x}}, \quad \Delta \mathrm{OP}_t = \alpha_0 + \alpha_1 \Delta C_t + \epsilon_t^{O}, \tag{2.12}$$

where $\epsilon_t^{\mathrm{x}} \sim N(0, \sigma_{\mathrm{x}}^2)$ and $\epsilon_t^{O} \sim N(0, \sigma_O^2)$, with the parameters calibrated via linear regression.

For future simulations, the following steps are undertaken. First, we obtain the simulated nominal market insurance catastrophe loss $\tilde{X}_t$ from the hazard module (see Section 2.2.2). Next, these insurance losses are scaled to represent uninsured economic damage, yielding $\eta \tilde{X}_t$. The production available for consumption after climate damage is then computed as:

$$C_t = Y_t - \eta \tilde{X}_t. \tag{2.13}$$

Subsequently, corporate earnings growth for the general sector is simulated based on Equation (2.12). For the brown sector, we apply a transition stress overlay factor (Grippa and Mann, 2020), which adjusts corporate earnings growth as:

$$\Delta \mathrm{OP}_t^B = \Delta \mathrm{OP}_t + \beta \Delta Y_t^B, \tag{2.14}$$

where ΔY_t^B represents the change in brown energy production, and β is the sensitivity of brown firms' corporate profits to these changes. Finally, the total excess return level is derived based on the simulated operating profit growth using Equation (2.12).

Based on the outputs from the interest rate (Section 2.3.2) and equity modules, investment returns are calculated as: $r_t^I = w_f \tilde{r}_t + (1 + w_f) r_t^{(S)}$, where w_f is the proportion of the portfolio allocated to risk-free assets.

In summary, the key inputs to this model are the nominal risk-free rate $\tilde{r}(t)$, aggregate catastrophe losses $\tilde{X}_t$, real GDP projections, and brown energy production for each SSP scenario (Y_t and Y_t^B), with $\tilde{r}(t)$ and $\tilde{X}_t$ obtained from the respective interest rate and hazards modules. The model outputs are the equity returns for the general portfolio, $r_t^{(S,G)}$, and for the brown portfolio, $r_t^{(S,B)}$. By preserving the simplicity of traditional methods while integrating forward-looking climate damage projections, this partial self-contained approach captures key trends in evolving climate and socio-economic conditions without using high-dimensional external factors.

Remark 2.6. *The current analysis considers only investments in the Australian market, effectively using Australian asset returns as a proxy for insurers' investment portfolio performance. In practice, however, insurers often hold exposure to foreign assets. This limitation is less concerning over a long-term horizon, as the SSP framework assumes convergence in economic growth across different countries (Dellink et al., 2017a). Moreover, persistent return differentials between markets are expected to diminish over time due to arbitrage. It is also worth noting that the asset model employed is deliberately simplified to align with the broader design of the framework, which prioritises scope and interpretability over granular modelling complexity.*

Another key assumption in the asset module is that short-term government bonds are considered free of default risk. This approach aligns with the risk-free treatment commonly adopted in conventional DFA studies (see, e.g., Kaufmann et al., 2001; D'Arcy and Gorvett, 2004; Consigli et al., 2018) and is consistent with APRA's Prescribed Capital Amount (PCA) framework for Australian sovereign bonds (APRA, 2023). However, this assumption may require reconsideration in light of potential climate-induced sovereign downgrades as climate-related damages escalate (Klusak et al., 2023). The extent of this climate influence on sovereign risk varies across the literature. For example, Cevik and Jalles (2022) found that climate-related effects on bond spreads are statistically significant primarily in developing countries, where the capacity to adapt to climate change is generally weaker, but not in developed countries. In contrast, Klusak et al. (2023) suggest that highly rated (developed) countries may experience more pronounced rating downgrades, though this may partly reflect the design of current rating methodologies. Additionally, Mallucci (2022) projects rising sovereign default probabilities and credit spreads as natural disasters intensify, though their focus is on small island nations with frequent hazard exposure, leaving the implications for developed economies less certain. Future studies could incorporate default risk into the modelling of government bond returns within DFA frameworks under climate change scenarios, leveraging existing findings to assess the potential material impact on the financial performance of general insurers.

2.4 Liabilities and premiums

2.4.1. Insurance costs

Drawing on the hazard module outputs (Section 2.2.2) and assuming an aggregate excess-of-loss reinsurance contract, the net catastrophe loss allocated to insurer j is determined by:

$$\tilde{X}_{t,(j)}^{\text{net}} = w_j\tilde{X}_t - \min((w_j\tilde{X}_t - d_{(j)})_+, L_{(j)}), \tag{2.15}$$

where $\tilde{X}_t$ represents the gross CAT losses, w_j denotes the market share of insurer j, and $d(j)$ and $L_{(j)}$ are the inflation and GDP-adjusted reinsurance excess and limit levels for insurer j. The second term in (2.15) represents the recoverables from reinsurers based on the excess-of-loss contract.

In addition to catastrophe losses, another key component of DFA liability modelling is non-catastrophe losses (Kaufmann et al., 2001). We model non-catastrophe losses with a Tweedie distribution (Jørgensen and Paes De Souza, 1994), which is a commonly used distribution assumption for modelling non-catastrophe loss. Specifically,

$$X_t^{\mathrm{NC}} \sim \mathrm{Tweedie}(\mu^{\mathrm{NC}}, \phi), \tag{2.16}$$

where μ^{NC} is the location parameter and ϕ is the dispersion parameter, both calibrated using historical data. Using a Tweedie distribution implies that claim frequency follows a Poisson distribution, while claim severity follows a Gamma distribution, reflecting the typically high-frequency, low-severity nature of non-catastrophe losses. Some studies have investigated the influence of weather on non-catastrophe claims (e.g., McGuire, 2008; Haug et al., 2011; Scheel et al., 2013; Reig Torra et al., 2023), but these typically require high-resolution daily or monthly municipal-level data, exceeding the usual granularity of DFA. Moreover, the long-term effect of weather on non-catastrophe claims is uncertain. For instance, McGuire (2008) found that same-day precipitation increases motor claims frequency, whereas lagged precipitation decreases it possibly due to cleaner road conditions (Eisenberg, 2004; McGuire, 2008). Consequently, we do not explicitly incorporate climate impacts in our modelling of non-catastrophe losses.

For projections, the aggregate non-catastrophe loss is computed as

$$\tilde{X}_{t,(j)}^{\mathrm{NC}} = X_t^{\mathrm{NC}} \cdot \omega_t \cdot w_j \cdot \frac{\mathrm{CPI}t}{\mathrm{CPI}s}, \tag{2.17}$$

where ω_t is the total number of risks, s denotes the reference year, and CPI_t is the climate-adjusted CPI from the inflation module (see Section 2.3.1). The total number of risks is modeled as a linear function of population:

$$\hat{\omega}_t = \hat{\omega}_0 + \hat{\omega}_1 \mathrm{Pop}_t, \tag{2.18}$$

where Pop_t is the projected population for each climate scenario, and the parameters $\hat{\omega}_0$ and $\hat{\omega}_1$ are calibrated on historical data via linear regression. Under these assumptions, climate change does not directly affect non-catastrophe losses; however, it still influences them indirectly through population growth and inflation.

Remark 2.7. *The exposure growth modelling presented here does not consider the potential loss of business volume due to premium increases driven by climate change. This simplification relies on the assumption that household income growth will generally keep pace with rising premiums. While this may be less concerning under scenarios such as SSP 8.5—where both economic growth and climate risk are high—or SSP 2.6—where climate risk is low—the issue of affordability may become more significant under scenarios with weak income growth but elevated climate risk (e.g., SSP 7.0). An initial effort to assess premium affordability in the context of climate change in Australia is being undertaken through the Insurance Climate Vulnerability Assessment project initiated by APRA in 2023 (Australian Prudential Regulation Authority, 2023), with results expected by the end of 2025. Future research could build on these findings to incorporate the impact of premium affordability on business volume.*

2.4.2. Insurance premiums

Based on the distribution assumptions of catastrophe and non-catastrophe losses, the insurance premium is then calculated using the standard deviations loading principle (Paudel et al., 2013, 2015; Tesselaar et al., 2020):

$$\pi_{t,(j)} = \underbrace{\mathsf{E}(\tilde{X}_{t,(j)}) + \rho\sqrt{\mathsf{Var}(\tilde{X}_{t,(j)})}}_{\text{CAT premium}} + \underbrace{\mathsf{E}(\tilde{X}^{\mathrm{NC}}_{t,(j)}) + \rho\sqrt{\mathsf{Var}(\tilde{X}^{\mathrm{NC}}_{t,(j)})}}_{\text{Non-CAT premium}}, \tag{2.19}$$

where ρ is the risk aversion parameter that reflects the level of insurer's risk aversion towards the extreme nature of the risk (Paudel et al., 2013). The risk aversion parameter could be selected empirically. We adopt the assumed risk aversion parameter of 0.55 in Kunreuther et al. (2011) and Paudel et al. (2013), which is based on an empirical survey analysis conducted by Kunreuther and Michel-Kerjan (2011). The implication of this assumption on the projected premiums growth will also be examined in Section 3.2.3.

2.4.3. Reinsurance premiums and cycles

Based on the reinsurance structure specified in Section 2.4.1, the reinsurance premium is derived as:

$$\pi^{RI}_{t,(j)} = \mathsf{E}[\min((\tilde{X}_{t,(j)} - d_{(j)})_+, L_{(j)})] + \rho\sqrt{\mathsf{Var}(\min((\tilde{X}_{t,(j)} - d_{(j)})_+, L_{(j)}))}. \tag{2.20}$$

Similarly, the second term in (2.20) represents the surcharge on the premium above the expected value of the loss, which is dependent on the variability of the reinsurance losses.

Since reinsurers typically cover the extreme tail of insurers' risk portfolios through excess-of-loss coverage, large natural catastrophes can strain reinsurance capital, potentially triggering a hard reinsurance market with higher premiums (Tesselaar et al., 2020). This effect is expected to intensify as climate change increases catastrophe losses (Tesselaar et al., 2020). One popular explanation of this phenomenon is the capital constraint theory, suggesting firms prefer to accumulate surplus internally (via higher premiums) rather than raising costly external capital, leading to persistence during the hard market phase (Winter, 1988, 1994; Dicks and Garven, 2022).

In conventional Dynamic Financial Analysis (DFA) applications, market cycles are often modelled using an AR(2) process (see, e.g., Cummins and Outreville, 1985; Boyer et al., 2012) or a Markov chain (see, e.g., Kaufmann et al., 2001; Eling et al., 2008). However, these approaches do not explicitly model the key process drivers of market cycles (e.g., capital level), which can be influenced by external environmental factors, particularly under the impacts of climate change across different scenarios. To address this limitation, we directly model the reinsurance premium as a function of reinsurance capital using a negative exponential function, inspired by the functional form in Taylor (2008):

$$\pi^{RI,*}_{t,(j)} = \max\left(\pi^{RI}_{t,(j)}, \pi^{RI}_{t,(j)} e^{-k_1\cdot(S_{t-1}-S_0)}\right), \tag{2.21}$$

where S_{t-1} denotes the solvency ratio at the end of period $t-1$, S_0 represents the reference (or steady-state) solvency ratio, and k_1 is the premium-to-solvency sensitivity parameter. The solvency ratio is defined as the ratio of reinsurance capital to premium (i.e., $S_{t-1} = K^{\mathrm{Re}}_{t-1}/\pi^{RI,*}_{t-1}$), where the reinsurance capital is derived as:

$$K^{\mathrm{Re}}_t = (1+\tilde{r}^{(I)}_t)\left(K^{\mathrm{Re}}_{t-1} + \sum_{j=1}^{J}\pi^{RI,*}_{t,(j)}\right) - \sum_{j=1}^{J}\min\left[(\tilde{X}_{t,(j)} - d_{(j)})_+, L_{(j)}\right]. \tag{2.22}$$

Here, we assume that reinsurers earn the same investment returns as direct insurers. The specification in (2.21) ensures that premiums increase as the solvency ratio decreases. Furthermore, due to the concave nature of the function, a decline in capital levels results in a more pronounced increase in premiums compared to the decrease in premiums when capital levels rise. This asymmetry aligns with the assumptions in Winter (1994), where insurers are assumed to be averse to the risk of bankruptcy.

Remark 2.8. *We acknowledge that the reinsurance cycle model presented here is a simplified representation, as it assumes a single reinsurer exclusively covering catastrophe losses in Australia. Despite its highly stylised nature, the model generally captures the inverse relationship between reinsurance capital and premium pricing dynamics. The impacts of climate change on the reinsurance cycle itself could be a separately interesting topic, and we will leave it for future research.*

2.5 Surplus and performance measures

Based on the simulated quantities from the previous module, the market surplus process is derived as (Kaufmann et al., 2001):

$$K_t = \sum_{j=1}^{J} K_t^{(j)} = \sum_{j=1}^{J} (1 + \tilde{r}_t^{(I)})(K_{t-1}^{(j)} + \tilde{\pi}_t^{(j)}) - (\tilde{X}_{t,(j)}^{\text{net}} + \tilde{X}_{t,(j)}^{\text{NC}}), \tag{2.23}$$

where $K_t^{(j)}$ represents the surplus for entity j at time t. Market insolvency is defined as $K_t < 0$.

To determine the initial capital level $K_0^{(j)}$, the base capital requirement $\tilde{K}_0^{(j)}$ is calibrated to satisfy $\Pr(K_1^{(j)} \leq 0) = 0.5\%$, consistent with the solvency standards under Solvency II (Christiansen and Niemeyer, 2014). Recognizing that insurers typically maintain capital buffers above the minimum required capital to mitigate insolvency risk, we scale this base requirement using a target capital ratio τ. Therefore, the final starting capital is thus computed as $K_0^{(j)} = \tau \tilde{K}_0^{(j)}$.

The financial performance of general insurers is typically evaluated using both returns and risk measures. For returns, we consider the median surplus $\text{med}(K_t)$ – the median of the surplus distribution at time t – alongside the expected surplus:

$$\text{E}(K_t) = \frac{1}{N} \sum_{n=1}^{N} K_t^{(n)}, \tag{2.24}$$

where N is the total number of simulations. These two measures are commonly used returns metrics in DFA studies (see, e.g., Kaufmann et al., 2001).

For the risk measures, we use both insolvency probability and the deficit-given-insolvency ratio. The insolvency probability, a common DFA risk metric (Kaufmann et al., 2001), is calculated as the proportion of simulations yielding zero or negative capital:

$$\text{P}(K_t < 0) = \frac{1}{N} \sum_{n=1}^{N} \mathbb{I}(K_t^{(n)} \leq 0). \tag{2.25}$$

The second measure we consider is the deficit-given-insolvency ratio, given by:

$$\text{E}\left[\frac{-K_t}{L_t} \mid K_t < 0\right], \tag{2.26}$$

where $L_t = \sum_{j=1}^{J} \tilde{X}^{\text{net}}_{t,(j)} + \tilde{X}^{\text{NC}}_{t,(j)}$ represents the total claims liabilities at time t. This ratio measures the severity of the market deficit conditional on insolvency and is analogous to the Loss-Given-Default (LGD) metric used in reinsurance credit risk (Chen et al., 2020). Together, these risk measures provide a comprehensive assessment of both the likelihood and severity of adverse outcomes in the surplus process.

3 Numerical results and discussions

After introducing the modelling framework for the climate-dependent DFA, this section presents numerical examples to demonstrate its application within the Australian general insurance market. Section 3.1 outlines the data sources and parameter calibrations used in the proposed framework. Section 3.2 analyses key simulation results from individual modules and discusses their potential financial implications for general insurers. Finally, Section 3.3 analyses and compares general insurers' financial performance under different climate scenarios using both risk and return measures.

3.1 Data and calibration

3.1.1. Data sources

Climate data

The historical weather data used to calibrate the climate and hazard modules are sourced from ERA 5 reanalysis data (Copernicus Climate Change Service, 2024b), which combines past observations with current weather computer models to provide consistent estimates of atmospheric, land and oceanic climate variables from 1950 to the present. For future projections, we use the outputs from the CMIP6 models (Copernicus Climate Change Service, 2024a), which offers projected meteorological variables under various emissions scenarios up to 2100 at both monthly and daily resolutions. Additionally, the CMIP6 models generate backcasts of climate variables from 1850 to 2014, which –together with historical data – are used to calibrate the bias correction and aleatoric uncertainty models as detailed in Section 2.2.1. As our analysis focuses on the frequency and severity of hazards at the national level, we use the average values of climate observations across all gridded cells for calibration and projection purposes.

Hazards data

To calibrate the frequency and severity models for catastrophe insurance losses as detailed in Section 2.2.2, we draw on the ICA dataset (Copernicus Climate Change Service, 2024c), which is maintained by the Insurance Council of Australia. This dataset covers all recorded natural disasters in Australia from 1967 to 2024, including variables such as disaster locations, start and end dates, and total insured damages.

Macro-economic data

In Section 2.3.2, we calibrate the interest rate model using the RBA cash rates data (Reserve Bank of Australia, 2024) and potential GDP growth estimates from the World Bank Potential Growth Database (Kilic Celik et al., 2023). The RBA dataset covers cash rate targets and overnight cash rates from 1976 to 2023, while the World Bank Database offers annual Australian potential GDP growth from 1981 to 2021. Consequently, the calibration period spans 1981–2021.

In Section 2.3.1, we calibrate the inflation rates model with data from Australian Bureau of Statistics (2024b), which provides quarterly Consumer Price Index (CPI) information for Australia from 1948 to 2023. These data are aggregated to an annual scale to align with the DFA model's time resolution.

For projections, we obtain socio-economic variables from the IIASA SSP database (Riahi et al., 2017), offering forecasts of GDP, population, and energy production at the five-year interval under multiple development paths at the country level. Spline interpolation (Erdogan, 2013) is then used to convert these projections to annual data.

Financial data

To calibrate the equity models described in Section 2.3.3, we employ Australian gross corporate operating profits and total returns data for the All-Ordinaries share index. The corporate operating profits dataset, sourced from Australian Bureau of Statistics (2024a), covers the total industry on a quarterly basis from 1994 to 2023. The All-Ordinaries index data, obtained from FactSet (2024), provides daily-to-annual total returns from 1992 to 2023.

Insurance market statistics

In addition to the data sources mentioned above, we draw on Australian insurance market statistics from the General Insurance Performance Statistics database (APRA, 2024b) and the General Insurance Institution-Level Statistics database (APRA, 2024a). These data inform our market assumptions and support the calibration of the non-catastrophe loss model (see Section 2.4.1). Because no direct non-catastrophe loss data are publicly available, we derive industry-level non-catastrophe losses by subtracting the ICA-recorded catastrophe losses from the total industry losses reported in the General Insurance Performance Statistics database (APRA, 2024a), after joining those two datasets.

The General Insurance Performance Statistics database contains quarterly aggregate financial data on Australian general insurers from 2002 to 2023, while the General Insurance Institution-Level Statistics database provides annual, institution-level financial information from 2005 to 2023. Both databases include key metrics such as insurance losses, premiums, equity bases, and the number of underwritten risks.

3.1.2. Calibration results

Due to the large number of parameters, the bias-correction and noise volatility parameters calibrated for selected climate variables in the climate module are presented in Appendix B for illustrative purposes.

Table 3.1 presents the calibrated parameters for the selected model of each hazard type [3]. The pool of candidate models from which these were chosen is detailed in Appendix C. Each final hazard model was selected on the basis of both the physical mechanisms discussed in Section 2.2.2 and relevant statistical measures. For instance, in Table B, all candidate flood frequency models exhibit positive coefficients for precipitation variables, which aligns with the physical processes behind pluvial and riverine flooding. Among these models, Model 3 (using `rx5day` as a proxy for extreme precipitation) demonstrates the best performance based on both AIC and BIC values, which are commonly used criteria in classical GLM regressions that consider both in-sample fit and model complexity (James et al., 2013). Additionally, the covariate coefficient in Model 3 is statistically significant at the 5% level. Hence, we select Model 3 as the final flood frequency model. As another example, even though the atmospheric temperature coefficient is not statistically significant at either the 5% or 10% levels, we retain it in the final model due to the importance of both atmospheric and near-surface temperature, and their potentially opposing effects on hailstorm frequency (see Section 2.2.2).

Hazards	Parameters	Values	Data (for calibration)	Data (for projection)
Flood	$\beta^{\text{rx5day}}_{(\lambda)}$	0.037**	ERA 5 re-analysis; ICA data	CMIP 6
	$\beta^{\text{rx5day}}_{(\mu)}$	0.035*	ERA 5 re-analysis; ICA data	CMIP 6
Bushfire	$\beta^{\text{mfwixx}}_{(\lambda)}$	0.084**	ERA 5 re-analysis; ICA data	CMIP 6
Cyclones	$\beta^{\text{SST}}_{(\lambda)}$	1.213***	ERA 5 re-analysis; ICA data	CMIP 6
Storms	$\beta^{\text{SST}}_{(\lambda)}$	0.348**	ERA 5 re-analysis; ICA data	CMIP 6
	$\beta^{\text{SST}}_{(\mu)}$	0.239	ERA 5 re-analysis; ICA data	CMIP 6
East Coast Low	$\beta^{\Delta\text{SST}}_{(\lambda)}$	2.189*	ERA 5 re-analysis; ICA data	CMIP 6
Hails	$\beta^{T^{\text{NS}}}_{(\lambda)}$	0.211***	ERA 5 re-analysis; ICA data	CMIP 6
	$\beta^{T^{\text{MT}}}_{(\lambda)}$	-0.079	ERA 5 re-analysis; ICA data	CMIP 6

+ $p < 0.1$, * $p < 0.05$, ** $p < 0.01$, *** $p < 0.001$

Table 3.1: Calibration of key parameters: Hazard modules

The calibrated parameters for the real risk-free interest rate and inflation rate models are shown in Table 3.2. The positive impact of potential GDP growth on real rates (as captured by the parameter β_1) aligns with the expectations discussed in Section 2.3.2. For temperature impacts on inflation, the coefficients α_{1+L} and β_{1+L} are taken from Kotz et al. (2024), who calibrated these parameters across 121 countries to evaluate climate-related effects on inflation.

Model	Parameters	Values	Data (for calibration)	Data (for projection)
Real rates	β_1 $(\partial r_t/\partial g_t)$	2.206**	RBA cash rate; World Bank Potential Growth Database	SSP database (IIASA)
	μ_r	-0.0005		
	ϕ_r	0.478		
	σ_r	0.025		
Inflation	α_{1+L}, β_{1+L}	—	(Kotz et al., 2024)	CMIP 6
	μ_i	0.0517	ABS CPI data	
	a_i	0.713	ABS CPI data	
	σ_i	0.0309	ABS CPI data	

Table 3.2: Calibration of key parameters: Macro-economic variables

The calibrated parameters for the equity model are shown in Table 3.3. The parameter α_1 (which shows the sensitivity of operating profit growth to the consumption growth) and σ_O (which shows the standard deviations of the operating profit growth) are calibrated based on the Australian operating growth data (Australian Bureau of Statistics, 2024a) and the consumption growth data (World Bank Group, 2024). The parameter β_1 (which shows the sensitivity of the excess equity returns to operating profit growth) and the parameter σ_X (which is the standard deviations of the excess equity returns) are calibrated based on the operating growth data (Australian Bureau of Statistics, 2024a) and the total returns data on All-Ordinaries index (FactSet, 2024). The results suggest a positive relationship between operating profit growth and consumption growth, and a positive relationship between operating profit growth and excess equity returns, which aligns with expectations as discussed in Appendix A.

To calibrate the sensitivity of operating profits in brown firms [4] to planned changes in production under various climate scenarios (sourced from the SSP database (Riahi et al., 2017)), we adopt a simplified approach akin to that used in Grippa and Mann (2020). We estimate the impact of changes in output on operating profits for a representative firm in the Australian energy sector by considering its fixed and variable costs. These results are then extrapolated to other oil and gas firms within the sector. Woodside Energy Group Ltd (WDS) is selected as the representative firm, given its dominant market share of 66% in the Australian energy sector as of March 2024 (FactSet, 2024). The impact of output changes is calculated as the average percentage change in operating profit per 1% change in production, based on the historical financial statements available from 2014 to 2021 in FactSet. While this approach is intentionally simplified, general insurers may refine it to better align with their portfolio compositions. Enhancements could include integrating more granular transition risk metrics, potentially incorporating proprietary data sources.

Parameters	Values	Data (for calibration)	Data (for projection)
α_1 $(\partial\triangle OP_t/\partial\triangle C_t)$	3.824*	World Development Indicators (World Bank);	SSP database (IIASA)
		ABS Business Indicators	CMIP 6
σ_O	0.083		
β_1 $(\partial x_t/\partial\triangle OP_t)$	0.047	ABS Business Indicators; All-Ordinaries index (Factset)	SSP database (IIASA)
σ_X	0.103		
$\beta^{(B)}$ $(\partial\triangle OP_t^B/\partial\triangle Y_t^B)$	1.768	Income statements of WDS (Factset)	SSP database (IIASA)

Table 3.3: Calibration of key parameters: Equity returns

Table 3.4 presents the market assumptions underlying our simulations, derived from general insurance market statistics (APRA, 2024c) and financial disclosures from individual insurers. In the projections, both excess and limit levels are adjusted for changes in GDP and CPI across future periods and under different climate scenarios.

Size of Insurers	Numbers	Market Shares	Excess (normalised)	Limit (normalised)
Large	4	20%	$1000 million	$600 million
Medium	4	3%	$150 million	$90 million
Small	12	0.67%	$33 million	$20 million

Table 3.4: Market assumptions

Table 3.5 summarises the additional assumptions used in the simulations. The target capital ratio is determined as the general insurance industry's average ratio of eligible equity to the Minimum Capital Requirement (MCR), based on data from the APRA General Insurance Institution-Level Statistics database (APRA, 2024a). The uninsured-to-insured loss ratio is used to scale catastrophe insurance losses from the hazard module to uninsured economic damage, serving as an input to the equity model. This ratio is calculated as the average proportion of uninsured to insured losses over the historical period from 1985 to 2023, using data from the EM-DAT database (EM–DAT, 2023), since the ICA dataset records only insurance losses.

Parameters	Type	Values	Source
ρ	Risk-aversion	0.55	Kunreuther et al. (2011); Paudel et al. (2013)
τ	Target capital ratio	1.75	APRA (2024a)
η	Uninsured-to-insured loss ratio	1.22	EM–DAT (2023)
w_{rf}	Allocation to risk-free assets	60% [5]	OECD (2023)
w_B	Allocation to brown assets	3%	Gatzert and Özdil (2024)

Table 3.5: Other assumptions

3.2 Key simulation results from individual modules

3.2.1. Climate and hazards

The simulated climate variables derived from the CMIP6 model outputs (Copernicus Climate Change Service, 2024a) are presented in Figure 3.1. In this figure, the solid lines represent the average simulation path, while the dashed lines indicate the 5^{th} and 95^{th} percentiles. The results suggest that most climate variables, except for SST gradients, exhibit an upward trend, particularly under high-emission scenarios, indicating an overall increase in climate risk.

In addition to this long-term trend, the average simulation path also shows notable inter-annual variability. This variability, likely driven by internal climate processes (e.g., El Niño cycles) captured by the CMIP6 models (Jain et al., 2023), may contribute to annual fluctuations in insurance premiums and costs as shown in later sections.

Furthermore, the projections display a high degree of uncertainty, as shown by the wide range between the 5^{th} and 95^{th} percentiles. This uncertainty, also highlighted in other studies (see, e.g., Wu et al., 2022), arises from both the climate model uncertainty and the aleatoric uncertainty incorporated in our climate module (see Section 2.2.1). Given that such uncertainty, especially at the upper percentiles, is crucial for actuarial applications and capital modelling, these findings underscore the importance of accounting for uncertainty in climate projections, as discussed in Section 1.2 and 2.2.1.

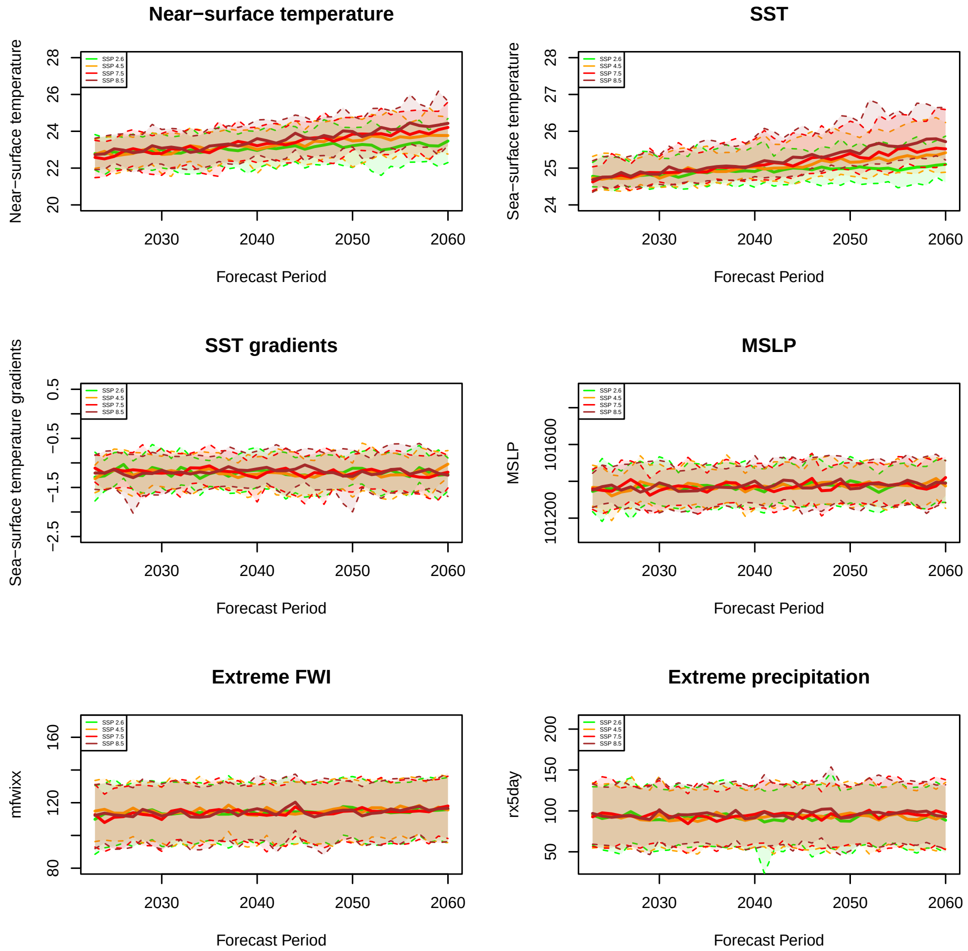

Figure 3.1: Simulation results of climate variables: Average simulation path (solid lines), 5^{th} and 95^{th} percentiles of simulations (dashed lines)

Based on the simulated climate variables, catastrophe losses for each hazard type are generated using the calibrated relationships between climate variables and hazard frequency and severity as described in Section 3.1.2. Overall, the projected normalised losses exhibit an increasing trend for most hazards, particularly under high-emission scenarios, with notable increases in both the mean and the upper tails of the loss distributions. Moreover, the results reveal considerable uncertainty, driven by both the variability in simulation of climate variables as shown in Figure 3.1 and the heavy-tailed nature of catastrophe losses. The rising mean and volatility are expected to place upward pressure on both insurance and reinsurance premiums, as well as shocks to capital over time.

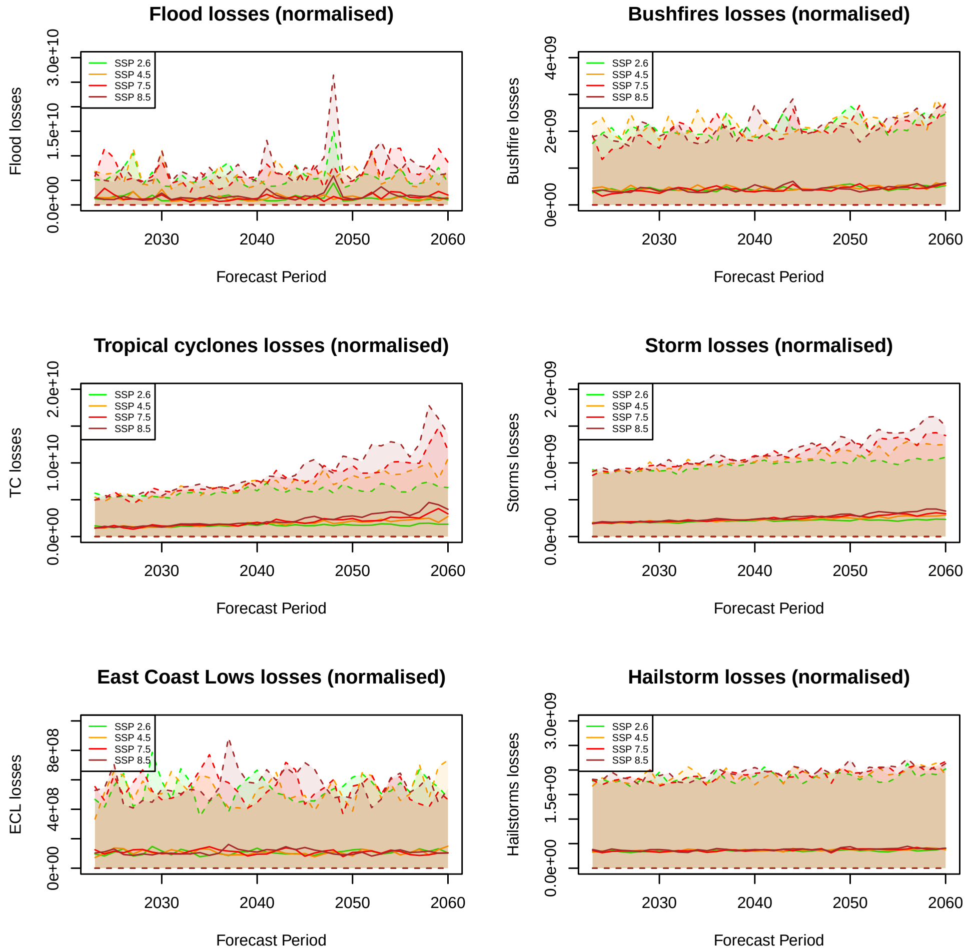

Figure 3.2: Simulation results of hazard losses (normalised): Average simulation path (solid lines), 5^{th} and 95^{th} percentiles of simulations (dashed lines)

Remark 3.1. *Despite the simplified structure of our hazard models, the simulation results generally align with trends in hazard risk based on physical mechanisms reported in the literature. The projected increases in losses from bushfires and floods are consistent with previous findings (IPCC, 2021a,b), reflecting the intensification of extreme fire weather across Australia and increased extreme precipitation in most regions. The rising losses from tropical cyclones and storms are primarily driven by increasing mean sea-surface temperatures, as illustrated in Figure 3.1 and based on the calibrated model described in Section 3.1.2.*

For tropical cyclones, existing literature suggests a decrease in the total number of cyclones but an increase in the frequency of high-intensity events (IPCC, 2021b). Since our frequency models rely on the ICA dataset, which only records hazards that result in catastrophe losses, the projected frequency reflects the number of catastrophe-level events (i.e., high-intensity tropical cyclones). Therefore, the increasing trend projected by our models is broadly consistent with findings in the literature.

Regarding hailstorms, although rising near-surface and atmospheric temperatures have opposing effects on storm dynamics, a net increase in losses is projected. This trend is attributed *to the stronger influence of near-surface temperature on storm frequency, as shown in Table 3.1, and aligns with the expected increases in hailstorm frequency in Australia (Leslie et al., 2008; Allen et al., 2014; Raupach et al., 2021).*

For East Coast Lows, a slight decreasing trend is observed in the simulations, driven by trends in sea-surface temperature gradients. This result is consistent with the existing studies, which suggest a decrease in the East Coast Low frequency particularly under the high-emission scenarios. (Pepler et al., 2016a,b; Speer et al., 2021).

However, our focus is on the general trends in hazard losses rather than their exact magnitudes, as this application example seeks to assess industry-wide patterns. For more granular decision-making at the corporate level, such as capital allocation and portfolio steering, general insurers can leverage proprietary claims data to tailor their hazard models to their specific portfolios.

3.2.2. Investment returns

The simulation results for the cumulative investment returns, presented on a logarithmic scale, are shown in Figure 3.3 [6]. The uncertainty bounds in the figure account for historical fluctuations in interest rates and equity returns, as well as the variability in climate-related damage to production available for consumption, as illustrated in Figure 3.5 and derived via (2.13).

The observed trends in cumulative investment returns are primarily driven by the economic growth assumptions underlying each SSP scenario (Figure 3.4). Under SSP 8.5, the highest cumulative investment return is projected, driven by its robust economic growth assumption (O Neill et al., 2017), followed by SSP 2.6. Conversely, SSP 7.0 exhibits the weakest cumulative investment return, influenced by both its slow economic growth assumptions and high catastrophe damages, in line with its narrative (O Neill et al., 2017). The relatively high investment returns under SSP 8.5 and SSP 2.6 are likely to accelerate capital accumulation. By contrast, the lower returns, coupled with high catastrophe losses in SSP 7.0 (see Figures 3.6 and 3.2), are expected to slow the pace of capital accumulation under this scenario.

Remark 3.2. *The projected damage ratios from our climate-dependent DFA model are also compared with estimates from existing literature; a detailed discussion can be found in Appendix D.*

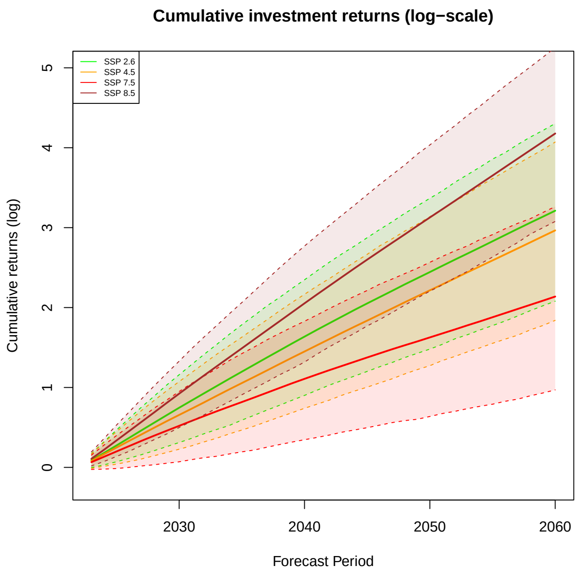

Figure 3.3: Simulated (log) compounded investment returns: Average simulation path (solid lines), 5^{th} and 95^{th} percentiles of simulations (dashed lines)

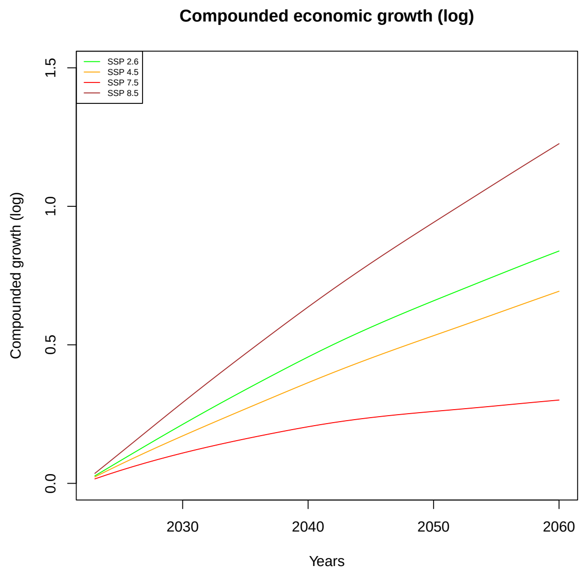

Figure 3.4: Compounded real GDP growth in Australia: derived from the SSP database (Riahi et al., 2017)

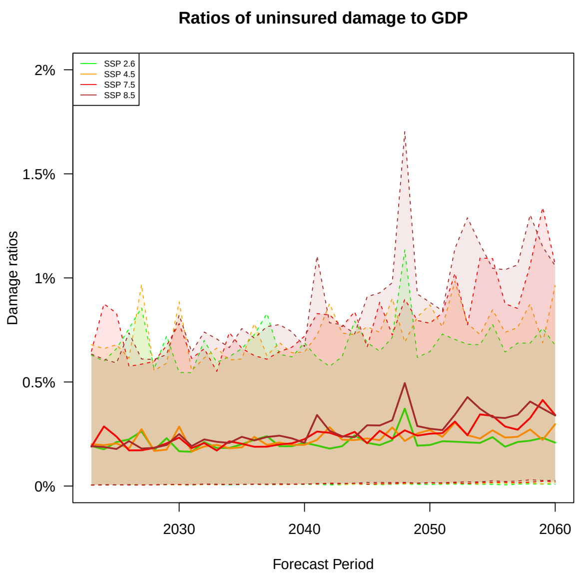

Figure 3.5: Ratios of uninsured catastrophe losses to GDP: Average simulation path (solid lines), 5^{th} and 95^{th} percentiles of simulations (dashed lines)

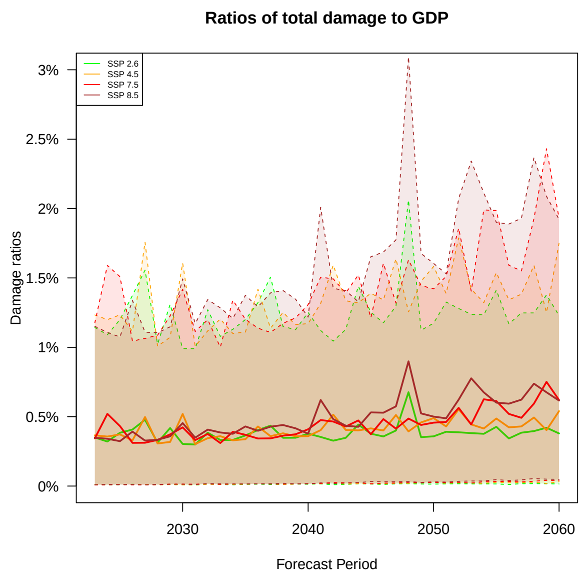

Figure 3.6: Ratios of total catastrophe economic damage to GDP: Average simulation path (solid lines), 5^{th} and 95^{th} percentiles of simulations (dashed lines)

3.2.3. Premiums and underwriting losses

The normalized gross premiums associated with catastrophe (CAT) coverage are presented in Figure 3.7. An overall increasing trend is found, driven by the rising risk of most hazards as shown in Figure 3.2. Gross CAT premiums reach their highest levels under SSP 8.5, particularly in the later projection period, followed by SSP 7.0, SSP 4.5, and SSP 2.6, in line with the physical risk narratives underlying those scenarios as described in Section 2.1. In addition to this general upward trend, significant inter-annual variability is observed, reflecting the internal climate variability of the underlying climate variables as shown in Figure 3.1.

Moreover, the proportion of CAT premiums relative to total general insurance premiums is expected to increase relative to the historical levels, with a more pronounced increase under high-emission scenarios. This is illustrated in Figure 3.8, which compares projected CAT premium proportions with historically observed CAT loss proportions (used here as a proxy for historical CAT premium proportions) derived from the General Insurance Performance Database (APRA, 2024c) and the ICA dataset. These findings suggest that catastrophe losses will have an increasingly significant impact on the underwriting performance of general insurers under the influence of climate change. Consequently, managing CAT exposures will become a more critical component of portfolio management for general insurers.

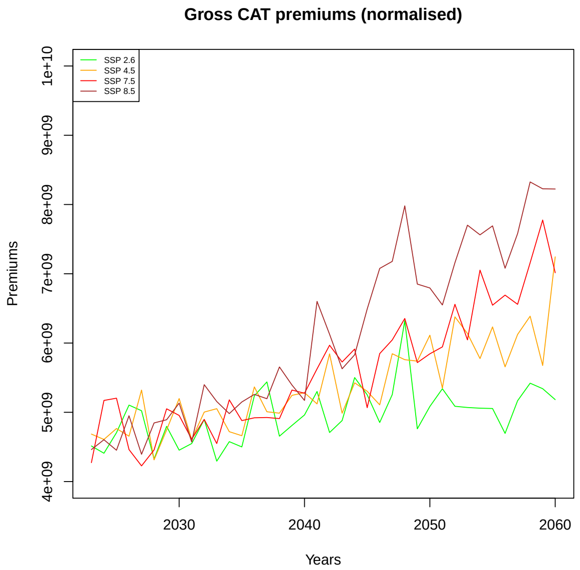

Figure 3.7: Gross premiums associated with catastrophe cover (normalised)

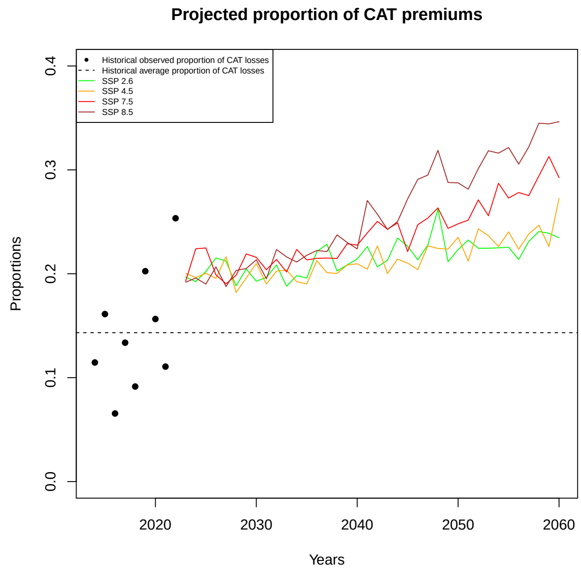

Figure 3.8: Projected proportion of CAT premiums and historical proportion of CAT losses

A similar pattern to the gross insurance premiums emerges in the reinsurance premiums (Figure 3.9), which show a general upward trend. The highest projected premium occurs under SSP 8.5, followed by SSP 7.0, while SSP 2.6 is expected to have the lowest premium.

To illustrate the role of reinsurance capital constraints, Figure 3.10 presents the average relative difference between the solvency-sensitive reinsurance premiums (in (2.20)) and the base premiums (in (2.21)). The largest uplift appears under SSP 7.0, likely due to low investment returns coupled with high insurance losses (Sections 3.2.1 and 3.2.2), resulting in slower capital accumulation and prolonged tight capacity. In contrast, SSP 8.5 exhibits the smallest uplift despite experiencing the highest catastrophe (CAT) losses, possibly because its stronger investment returns (see Section 3.2.2) accelerate capital accumulation and shorten tight-capacity periods. A similar pattern is also observed in the primary general insurance market (see Section 3.3).

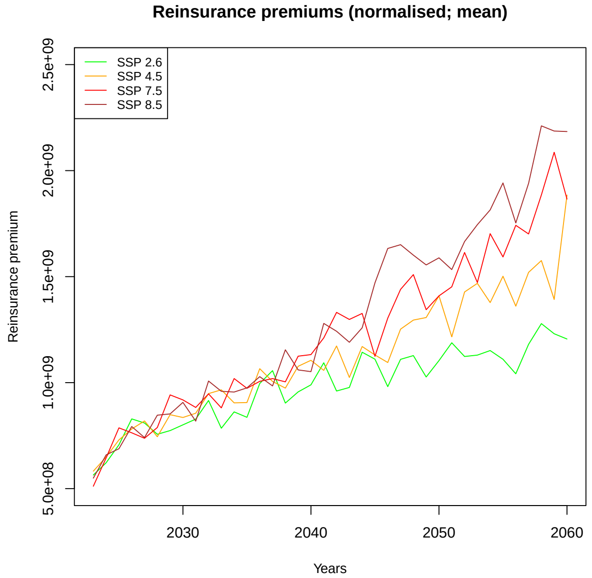

Figure 3.9: Reinsurance premiums (normalised; mean)

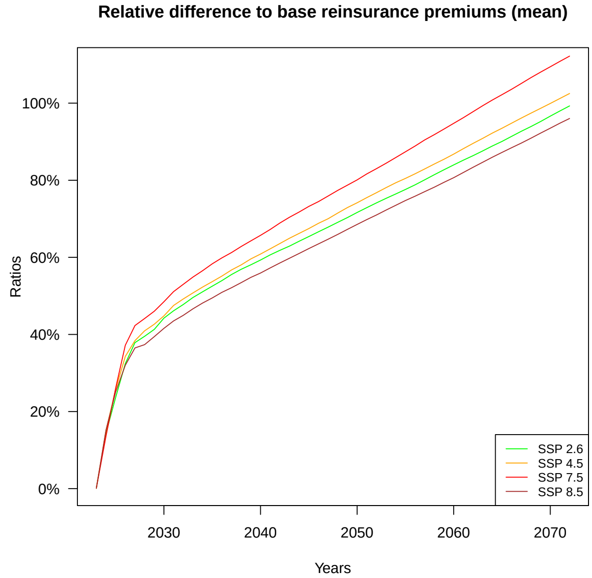

Figure 3.10: Relative difference between reinsurance premium (solvency-sensitive) and base reinsurance premium

Using the calculated premiums and simulated catastrophe losses from the hazard module (Section 3.2.1), we derive the simulated underwriting losses, with normalized results presented in Figure 3.11. On average, the simulated underwriting loss remains below zero (indicating a positive underwriting profit) and is relatively consistent across scenarios, which could be explained by the premium loadings. At higher quantiles, however, underwriting losses remain similar across scenarios initially but rise substantially in later periods under high-emission pathways (SSP 8.5 and SSP 7.0) due to escalating climate risks. This upward shift in the tail of underwriting losses can be attributed to the increasing volatility and extreme percentile of hazard losses observed under high-emission scenarios (see Section 3.2.1). Consequently, while downside liability impacts on financial performance appear moderate at first, they are expected to intensify over longer projection horizons in the high-emission scenarios.

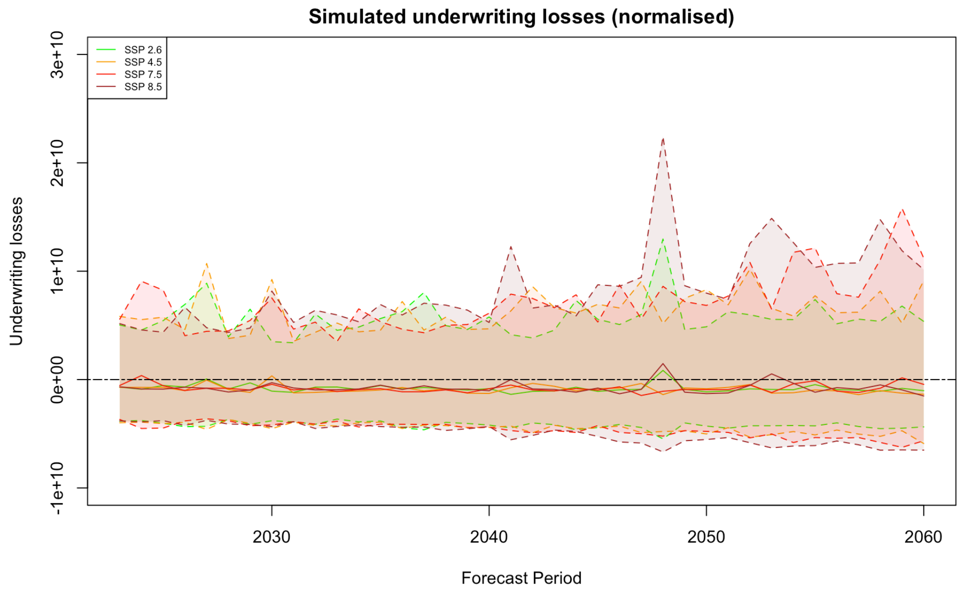

Figure 3.11: Simulations of underwriting losses (normalised)

3.3 Risk and returns measures

Finally, the risk and return measures for the general insurance market can be derived from the surplus, which is calculated using outputs from the individual modules (see (2.23)). Figures 3.12 and 3.13 show the expected and median surplus, which are our return measures, across different SSP scenarios. Under SSP 8.5, surplus is highest, followed by SSP 2.6, whereas SSP 7.0 yields the lowest surplus.

To investigate the drivers of these surplus trends, Figures 3.14 and 3.13 compare the expected and median surplus with cumulative investment returns at their average and median paths, revealing that differences in cumulative investment returns largely explain the observed surplus patterns. These findings align with earlier results showing that underwriting profits or losses are similar at mean levels across scenarios (Section 3.2.3), making investment growth the primary driver of mean and median surplus trends. Since investment returns are predominantly affected by the economic growth assumptions underlying each scenario (Section 3.2.2), the divergent economic growth paths in different SSP scenarios are expected to be the key drivers of expected returns to the general insurance industry.

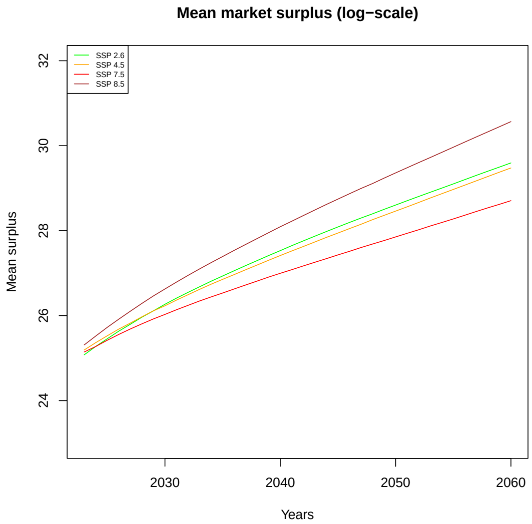

Figure 3.12: Expected market surplus (log-scale)

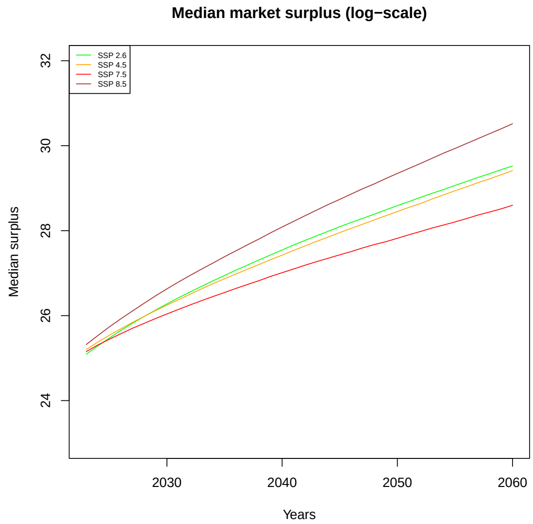

Figure 3.13: Median market surplus (log-scale)

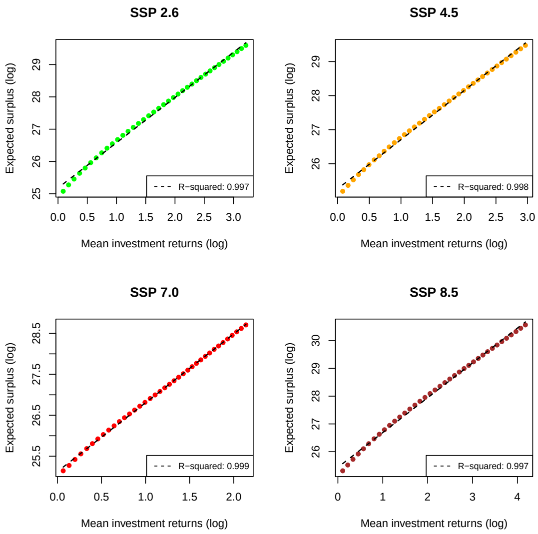

Figure 3.14: Expected market surplus (log-scale) v.s Average compounded investment returns (log-scale)

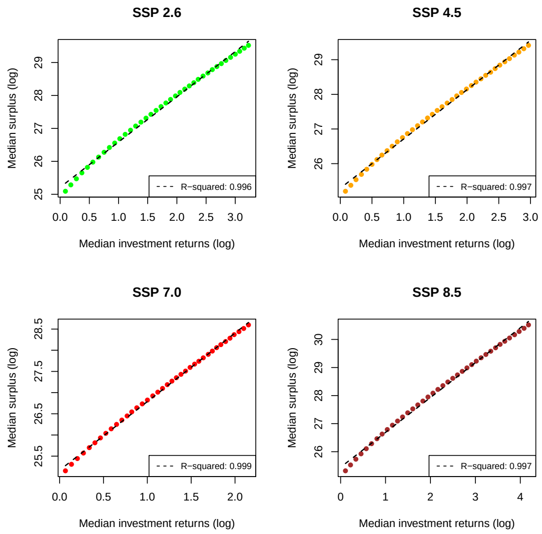

Figure 3.15: Median market surplus (log-scale) v.s Median compounded investment returns (log-scale)

Figure 3.16 shows market insolvency probabilities under various scenarios, a common risk metric in DFA studies (Kaufmann et al., 2001). SSP 7.0 exhibits the highest insolvency rates, followed by SSP 4.5 and SSP 2.6. Although SSP 7.0 does not incur the highest hazard losses, its poor investment returns (Section 3.2.2), substantial reinsurance premium increases (Section 3.2.3), and relatively high catastrophe (CAT) losses (Section 3.2.1) collectively erode profits and constrain capital accumulation, leading to high insolvency probabilities once both physical and economic aspects of the climate change are considered. These outcomes align with the physical and economic narratives underlying the SSP 7.0 scenario (Section 2.1).

Interestingly, although SSP 8.5 is generally associated with the highest physical risk in climate science literature (e.g., IPCC, 2021a), it yields the lowest projected insolvency probabilities once both physical and economic factors are considered into the modelling of general insurers' assets and liabilities. This may be attributed to stronger investment returns, driven by robust economic growth under the SSP 8.5 scenario, outpacing underwriting loss growth in the early projection horizon (see Figures 3.3 and 3.11). As a result, capital accumulates more rapidly, particularly over the early projection horizon. Indeed, Figure 3.18 indicates that SSP 8.5 exhibits the highest average Compound Annual Growth Rate (CAGR) of market surplus [7], which could help insurers absorb potential losses at later stages. These findings align with the SSP 8.5 narrative of "robust economic growth", which leads to "low adaptation challenges" except in extreme case (O Neill et al., 2017).

However, when insolvency does occur, SSP 8.5 incurs the most severe impact in later projection horizons, as indicated by the market deficit-given-insolvency ratios (Figure 3.17). These ratios, which also represent the proportion of claims unable to be paid to policyholders when insolvency occurs, imply that policyholders face the greatest losses under SSP 8.5 in tail events. This outcome likely arises from higher underwriting losses in the distribution tails under SSP 8.5, especially later in the projection period (Section 3.2.3; Figure 3.11), despite relatively small differences in early-horizon underwriting losses across scenarios. Moreover, given the limitations of the SSP 8.5 scenario assumptions discussed in Section 2.1, insurers should also be mindful of the potential for economic collapse triggered by climate tipping points, though it is not currently reflected in the scenario's underlying economic assumptions.

SSP 2.6 presents a more balanced risk-return profile, characterised by the second-highest expected surplus, second-lowest insolvency risk, and relatively small market deficits in insolvency. Additionally, catastrophe-related insurance and reinsurance premiums are expected to be the lowest under this scenario, which could potentially improve affordability and expand insurance coverage to protect society against climate risks. These findings align with SSP 2.6's narrative of "sustainable economic development" and "improving environmental conditions", which contribute to "low mitigation and adaptation challenges" (O Neill et al., 2017).

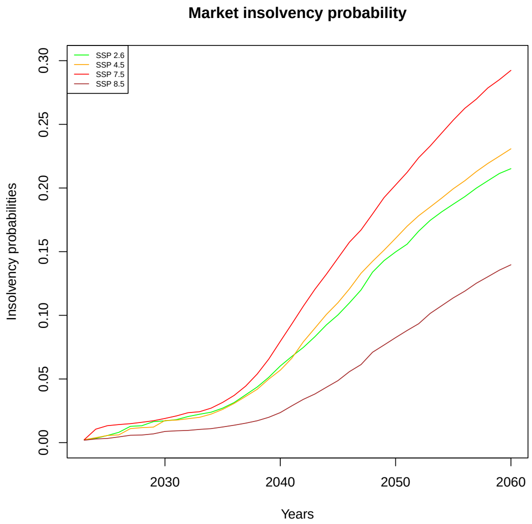

Figure 3.16: Market insolvency probabilities

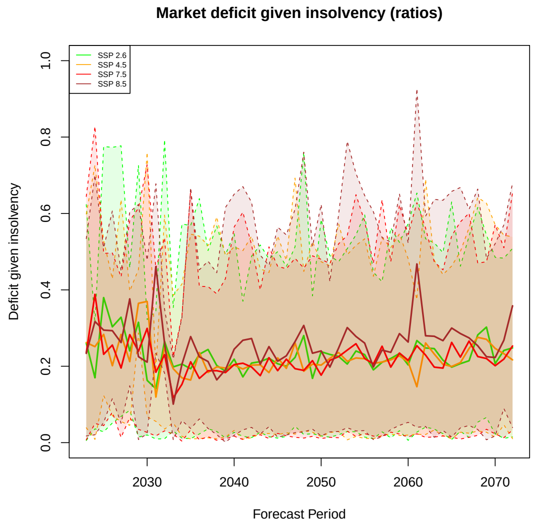

Figure 3.17: Market deficit-given-insolvency ratios [8]

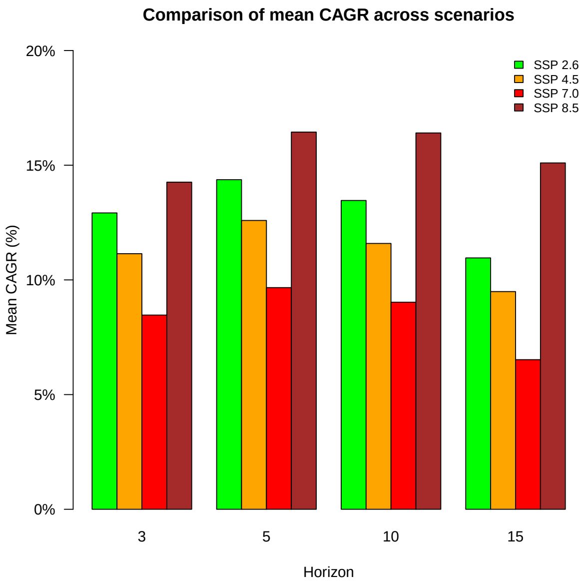

Figure 3.18: Mean Compound Annual Growth Rate (GACR) of market surplus, by projection horizons and climate scenarios

4 Conclusions

This study makes two key contributions. First, we propose a climate-dependent DFA framework that integrates climate risk into traditional Dynamic Financial Analysis. While previous studies examine the impacts of climate change on assets and liabilities separately, a unified framework remains underexplored. General insurers commonly use DFA to assess overall financial performance, yet conventional models do not account for climate risk. Our framework addresses this gap by leveraging the interconnected structure of DFA to capture the complex interactions of climate impacts on both assets and liabilities. Additionally, it incorporates a multi-year perspective to reflect the long-term nature of climate change. The uncertainty surrounding climate risks is addressed through stochastic simulations within climate scenario analysis, enabling the assessment of both risk and return dimensions. Finally, by incorporating the unique characteristics of general insurers, our framework provides realistic insights into the financial consequences of climate change on the insurance market.

Second, we conduct an extensive empirical study to assess the long-term impact of climate change on the Australian general insurance market, demonstrating the practical application of our framework. In climate science literature, SSP 8.5 is typically associated with the highest physical risk, followed by SSP 7.0, SSP 4.5, and SSP 2.6 (IPCC, 2021a). Our hazard simulations and CAT premium projections align with this ranking. However, when both economic and physical dimensions of climate scenarios are considered in relation to insurers' assets and liabilities, we find that SSP 7.0, characterised by high physical risk and poor economic growth, is the most detrimental scenario for insurers, leading to the lowest returns and highest insolvency risk. In contrast, SSP 8.5 yields the highest returns and lowest insolvency risk due to strong economic growth, but it also results in the largest market deficit in insolvency, posing significant risks to policyholders. These findings underscore the importance for general insurers to prepare for scenarios combining high catastrophe risk with weak economic growth in their critical strategic decisions, such as business planning, capital management, and reinsurance strategies. Additionally, insurers should be prepared for the tail-end financial repercussions of climate risk, particularly under high-emission scenarios such as SSP 8.5. Regulators, in turn, should ensure that insurers maintain sufficient capital buffers to withstand losses under different climate pathways and collaborate with governments to establish contingency plans, such as bail-out mechanisms, to mitigate systemic risks arising from the insolvency of major insurers.

5 Limitations and extensions

5.1 Reliances and limitations

By necessity, the modelling framework presented in this study relies on several simplifying assumptions to address the complexity and scale of climate risk. While this approach provides a practical starting point, it introduces several important limitations that could be addressed in future research.

Firstly, our analysis relies on the economic and environmental assumptions embedded in the SSP scenarios. As noted in Remark 2.1, these assumptions have several inherent limitations. Validating and refining these assumptions, and assessing their implications for general insurers, presents a valuable direction for future research and may require interdisciplinary collaboration among economists, climate scientists, and actuaries.

Secondly, our hazard loss forecasts are based on historically calibrated relationships between climate variables and observed insurance losses, which may change in the future. Future research could adopt a more forward-looking approach to account for these potential changes, as noted in Remark 2.4.

Thirdly, our framework is limited to disasters occurring within Australia and does not account for global spillover effects. As highlighted by (Neal et al., 2025), climate-induced economic damage can propagate across borders through international trade. Modelling such global linkages would provide a more comprehensive assessment of climate and market risks faced by local insurers.

A final limitation of our framework, as noted in Remark 2.7, is that it does not account for the potential loss of business volume resulting from rising premiums due to climate change. Addressing this aspect in future research could provide a more comprehensive assessment of long-term financial impacts on general insurers.

5.2 Extensions and future work

Our framework also offers several promising avenues for extension. First, this study focuses on assessing climate risks at an industry-wide level, serving as a starting point for integrating climate considerations into DFA frameworks. Building on the general framework proposed here, individual insurers could develop tailored, firm-level climate-dependent DFA models aligned with their specific risk profiles and exposure characteristics.

Second, as discussed in Remark 2.3, the model presented here serves as a baseline for measuring climate impacts without policy interventions. Future studies could assess the impacts of regulatory measures against the baseline to evaluate the effectiveness of different regulatory approaches across a range of climate scenarios.

Finally, the modelling approach adopted in this study is intentionally broad but relatively simplified. Future studies could consider more advanced component models to improve precision or address specific analytical needs. For example, incorporating proprietary catastrophe (CAT) models could provide more granular hazard modelling, while adding foreign investments and default risk assessments could strengthen the asset module, as noted in Remark 2.6. However, these enhancements should be carefully weighed against the trade-off between model complexity and parsimony, which is a key consideration in DFA applications.

Data and Code

The R code used to generate the results in this paper is available at `https://github.com/agi-lab/climate-dependent-DFA`. The datasets supporting the findings of this study are stored separately at `https://zenodo.org/records/15098758`. Detailed instructions for data access and code execution are provided on the linked GitHub page.

Due to licensing restrictions, we are unable to provide the Total Returns series of the All-Ordinaries Shares Index. Users are encouraged to obtain this data directly from FactSet. For those without a FactSet subscription, we provide pseudo data for model calibration, simulated from the calibrated equity model.

Similarly, we cannot distribute the financial statements of Woodside Energy Limited obtained from FactSet for the period 2014–2023. Users may access this data via FactSet or alternatively compile it manually from publicly available financial reports at `https://www.woodside.com/investors/reports-investor-briefings`. For models calibrated using these non-public datasets, we have applied the same parameters derived from the original data in the code to ensure consistency with the simulation results presented in this paper.

Acknowledgements

The views and opinions expressed in this paper are solely those of the authors and do not reflect those of their affiliated institutions.

The authors would like to extend their sincere gratitude to Sharanjit Paddam for his constructive feedback and insightful comments, which significantly improved the quality of this paper and provided valuable guidance for potential future research directions.

Earlier versions of this paper were presented at the 2024 Australasian Actuarial Education and Research Symposium (AAERS) and at research seminars hosted by the School of Risk and Actuarial Studies at UNSW. The authors are grateful for constructive comments received from colleagues who attended those events.

Declarations of interest

None

Notes

[1]The per-event normalised loss is defined as: $X_t^{(i),m} = \tilde{X}_t^{(i),m} \cdot \frac{\text{CPI}_s}{\text{CPI}_t} \cdot \frac{\text{Real GDP}_s}{\text{Real GDP}_t}$, which adjusts the nominal loss ($\tilde{X}_t^{(i)}$) for both the price level and total wealth in reference year s. Although our normalization technique is relatively simple, it aligns with conventional approaches in the literature (see, e.g., Pielke and Landsea, 1998; Vranes and Pielke Jr, 2009). While more granular factors could be incorporated into normalization (see, e.g., Crompton and McAneney, 2008; Pielke, 2021), our focus on future projections rather than historical trends – and on national-level rather than granular losses – supports the adoption of a more parsimonious approach.

[2]Note: The cyclone basin refers to the area of tropical cyclone formation.

[3]The notation in the table represents the coefficient associated with the climate variable (indicated as a superscript of β) for a specific distribution parameter (indicated as a subscript of β). For example, $\beta_{(\lambda)}^{\text{rx5day}}$ reflects the sensitivity of the frequency parameter (λ) to changes in `rx5day`, while $\beta_{(\mu)}^{\text{rx5day}}$ shows the sensitivity of the location parameter of the severity distribution to changes in `rx5day`.

[4]Here, we define brown firms as those operating within the oil and gas sector.

[5]The assumption is that the majority of bonds are invested in risk-free government securities, as insurers typically prefer government bonds over corporate bonds (OECD, 2023). Additionally, cash and deposits are considered nearly risk-free assets

[6]Here, the log-scale cumulative investment return is defined as: $r_t^{\text{cum}} = \log\left(\prod_{s=1}^{t}(1+r_s)\right)$. This can also be written as: $r_t^{\text{cum}} = \log\left(\prod_{s=1}^{t}(1+r_s)\right) = \log\left(\frac{V_0\prod_{s=1}^{t}(1+r_s)}{V_0}\right) = \log\left(\frac{V_t}{V_0}\right)$, where V_t is the total investment value at time t.

[7]The Compound Annual Growth Rate (CAGR) of the insurance surplus over the projection horizon T_h is given by: $\text{CAGR}_h = \left(\frac{K_{T_h}}{K_0}\right)^{\frac{1}{T_h}} - 1$. This measure, commonly used in finance to assess the average growth rate of an investment portfolio (Grimm, 2023), is employed here to evaluate the rate of capital accumulation across different projection horizons.

[8]Note that the market deficit-given-insolvency ratio exhibits high volatility across all climate scenarios in the early projection horizon. This is likely due to the relatively small number of simulation paths that become insolvent at early stages (see Figure 3.16), which leads to greater fluctuation in the calculated ratios.

A Equity models: supplementary details

In Section 2.3.3, equity returns are modelled as a function of operating profit growth, which in turn is modelled as a function of consumption growth. In this section, we examine the validity of this modelling assumption.

Dividend growth is a critical driver of total equity returns (see, e.g., Lettau and Ludvigson, 2005). The total dividends paid by corporations can be expressed as:

$$D_t = (\beta_t(1 - \text{Tax}_t)\zeta_t)C_t, \tag{A.1}$$

where β_t is the share of corporate's operating profits in the total economy at time t, Tax_t is the tax rate, and ζ_t is the dividend payout ratio at time t. Consequently, dividend growth is given by:

$$\Delta d_t = \frac{(\beta_t(1 - \text{Tax}_t)\zeta_t)C_t}{(\beta_{t-1}(1 - \text{Tax}_{t-1})\zeta_{t-1})C_{t-1}} - 1. \tag{A.2}$$

If the share of corporate operating profits, tax rates, and dividend payout ratios remain constant over time, dividend growth would be equal to consumption growth.

However, this assumption may be too restrictive. Instead of assuming a constant dividend payout ratio, we allow its change to be relatively constant over time (i.e., $1 + \Delta\zeta_t = \zeta_1 + \epsilon$, with $\epsilon \sim N(0, \sigma^2)$), then the change in dividend growth could be written as a linear function of the operating profit growth:

$$\Delta d_t = \zeta_0 + \zeta_1 \Delta\text{OP}_t + \tilde{\epsilon}_t, \tag{A.3}$$

where ΔOP_t is the change in operating profits defined as $\text{OP}_t = \beta_t(1 - \text{Tax}_t)C_t$. This formulation is analogous to our empirical model specified in (2.12).

Furthermore, the change in operating profit can be expressed as a function of consumption growth:

$$\Delta\text{OP}_t = (1 + \Delta\gamma_t)\Delta C_t + \Delta\gamma_t, \tag{A.4}$$

where $1 + \Delta\gamma_t = (1 + \Delta\beta_t)(1 + \Delta(1 - \text{Tax}_t))$. Assuming that the changes in the proportion of corporate profits to total consumption (i.e., $\Delta\beta_t$) and in tax rates (i.e., $\Delta(1 - \text{Tax}_t)$) are relatively constant over time, the change in operating profit can be modelled as a linear function of consumption growth:

$$\Delta\text{OP}_t = \alpha_0 + \alpha_1 \Delta C_t + \tilde{\epsilon}_t, \tag{A.5}$$

which is consistent with our empirical model in (2.12). As shown in Figure A, the assumption of a constant change in tax rates is supported by historical data, with Australian corporate tax rates remaining at 30% since 2002. Moreover, the proportion of corporate earnings is relatively stable over time, as demonstrated in Figure B.

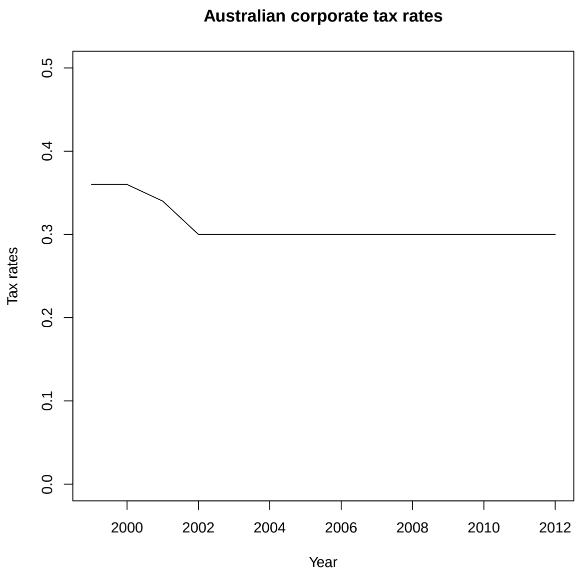

Figure A: Australian corporate tax rates (Data source: Trading Economics (2024)

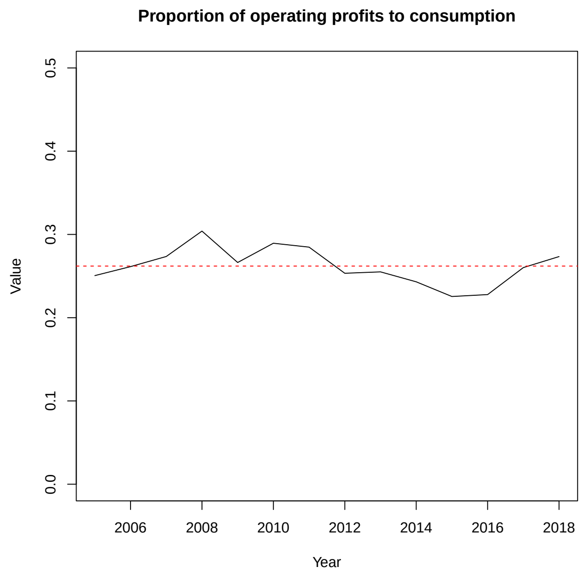

Figure B: Proportion of aggregate Australian corporate operating profits to total consumption in Australia (Data source: Australian Bureau of Statistics (2024a))

B Detailed calibration results for climate modules

Model names	$\hat{\beta}_0^{(m)}$	$\hat{\beta}_1^{(m)}$	$\hat{\sigma}_{(m)}$
ACCESS-CM2	2.257	0.883	1.271
CanESM5-CanOE	2.484	0.889	1.354
CESM2	-0.065	0.987	1.256
CMCC-CM2-SR5	-2.18	1.085	1.405
CNRM-CM6-1	0.735	0.974	1.321
CNRM-ESM2-1	0.868	0.942	1.186
FGOALS-f3-L	0.944	0.98	1.294
FGOALS-g3	-1.132	1.039	1.23
INM-CM4-8	1.345	0.971	1.199
INM-CM5-0	2.222	0.948	1.195
IPSL-CM6A-LR	-0.139	1.055	1.428
MCM-UA-1-0	1.329	0.899	1.401
MIROC-ES2L	-2.734	1.045	1.255
MIROC6	-0.85	0.931	1.325
MPI-ESM1-2-LR	1.441	0.916	1.288
MRI-ESM2-0	-0.046	0.96	1.375
NorESM2-MM	-0.858	1.036	1.267

Table A: Near-surface temperature (monthly-average): Calibrated bias-correction coefficients ($\hat{\beta}_0^{(m)}$ and $\hat{\beta}_1^{(m)}$), and standard deviation of noise ($\hat{\sigma}_{(m)}$)

Model names	$\hat{\beta}_0^{(m)}$	$\hat{\beta}_1^{(m)}$	$\hat{\sigma}_{(m)}$
ACCESS-CM2	0.926	1.045	1.622
CanESM5-CanOE	-4.122	0.924	1.32
CESM2	-4.897	0.881	1.491
CNRM-CM6-1	6.783	1.04	1.412
CNRM-ESM2-1	5.617	1.025	1.366
INM-CM4-8	12.879	1.361	1.346
INM-CM5-0	14.56	1.384	1.502
IPSL-CM6A-LR	1.294	1.001	1.409
MCM-UA-1-0	-0.307	0.982	1.368
MIROC-ES2L	-10.139	0.675	1.488
MIROC6	-4.526	0.86	1.369
MPI-ESM1-2-LR	1.847	1.036	1.475
MRI-ESM2-0	3.861	1.102	1.448
NorESM2-MM	-6.233	0.838	1.408
UKESM1-0-LL	2.097	1.066	1.596

Table B: Air temperature (monthly-average): Calibrated bias-correction coefficients ($\hat{\beta}_0^{(m)}$ and $\hat{\beta}_1^{(m)}$), and standard deviation of noise ($\hat{\sigma}_{(m)}$)

Model names	$\hat{\beta}_0^{(m)}$	$\hat{\beta}_1^{(m)}$	$\hat{\sigma}_{(m)}$
ACCESS-CM2	-2.418	0.996	0.316
CNRM-CM6-1	4.446	0.801	0.263
FGOALS-f3-L	2.266	0.924	0.35
FGOALS-g3	0.792	0.955	0.279
INM-CM4-8	1.414	0.944	0.239
INM-CM5-0	0.636	0.994	0.255
MCM-UA-1-0	2.26	0.881	0.378
MIROC-ES2L	-5.092	1.204	0.356
UKESM1-0-LL	1.157	0.943	0.262

Table C: Sea-surface temperature (monthly-average): Calibrated bias-correction coefficients ($\hat{\beta}_0^{(m)}$ and $\hat{\beta}_1^{(m)}$), and standard deviation of noise ($\hat{\sigma}_{(m)}$)

Model names	$\hat{\beta}_0^{(m)}$	$\hat{\beta}_1^{(m)}$	$\hat{\sigma}_{(m)}$
ACCESS-CM2	-17.133	1.306	8.675
ACCESS-ESM1-5	-4.806	1.239	8.346
CanESM5	-0.279	1.234	9.263
CMCC-CM2-SR5	57.288	1.052	7.644
CMCC-ESM2	53.705	0.959	10.141
EC-Earth3	-45.561	1.726	8.791
FGOALS-g3	8.191	1.323	8.697
GFDL-ESM4	5.471	1.261	8.534
INM-CM4-8	17.222	1.582	9.137
INM-CM5-0	-9.668	1.898	8.932
IPSL-CM6A-LR	42.053	1.074	8.376
KACE-1-0-G	-35.045	1.209	8.592
MIROC6	30.162	0.911	9.741
MPI-ESM1-2-HR	-42.055	1.476	8.781
MPI-ESM1-2-LR	-23.581	1.359	8.883
MRI-ESM2-0	-20.99	1.108	8.844
NorESM2-MM	40.105	0.992	8.963
TaiESM1	50.755	1.001	9.536

Table D: Fire Weather Index: Calibrated bias-correction coefficients ($\hat{\beta}_0^{(m)}$ and $\hat{\beta}_1^{(m)}$), and standard deviation of noise ($\hat{\sigma}_{(m)}$)

Model names	$\hat{\beta}_0^{(m)}$	$\hat{\beta}_1^{(m)}$	$\hat{\sigma}_{(m)}$
ACCESS-CM2	2471.323	0.975	146.064
CanESM5-CanOE	18345.06	0.819	136.658
CESM2	14433.794	0.857	154.145
CMCC-CM2-SR5	14248.639	0.859	144.904
CNRM-ESM2-1	2981.637	0.97	144.572
INM-CM4-8	-12552.876	1.125	133.775
INM-CM5-0	-25169.454	1.25	145.112
MCM-UA-1-0	37431.853	0.629	125.137
MIROC-ES2L	6250.218	0.942	179.028
MIROC6	624.259	0.998	169.48
MPI-ESM1-2-LR	-8807.205	1.087	170.452
MRI-ESM2-0	-23938.494	1.234	185.582
NorESM2-MM	15219.903	0.85	155.486
UKESM1-0-LL	10695.377	0.894	142.076

Table E: Mean sea-level pressure (MSLP): Calibrated bias-correction coefficients ($\hat{\beta}_0^{(m)}$ and $\hat{\beta}_1^{(m)}$), and standard deviation of noise ($\hat{\sigma}_{(m)}$)

Model names	$\hat{\beta}_0^{(m)}$	$\hat{\beta}_1^{(m)}$	$\hat{\sigma}_{(m)}$
access-cm2	2.811	1.156	18.276
access-esm1-5	4.2	1.051	17.659
bcc-csm2-mr	-22.791	1.417	20.799
canesm5	-12.108	1.517	18.868
cmcc-esm2	6.167	1.007	19.607
ec-earth3	-12.368	1.2	19.394
gfdl-esm4	-14.868	1.321	16.222
inm-cm4-8	11.73	0.985	18.008
inm-cm5-0	3.857	1.115	18.983
ipsl-cm6a-lr	-5.697	1.305	17.26
kace-1-0-g	16.459	0.953	16.631
miroc6	-45.993	1.728	19.952
mpi-esm1-2-hr	14.079	0.875	17.57
mpi-esm1-2-lr	-3.133	1.185	17.843
mri-esm2-0	20.245	0.835	16.37
noresm2-lm	-19.198	1.364	18.09
noresm2-mm	-17.776	1.263	18.665

Table F: Largest five-day cumulative precipitation (rx5day): Calibrated bias-correction coefficients ($\hat{\beta}_0^{(m)}$ and $\hat{\beta}_1^{(m)}$), and standard deviation of noise ($\hat{\sigma}_{(m)}$)

Model names	$\hat{\beta}_0^{(m)}$	$\hat{\beta}_1^{(m)}$	$\hat{\sigma}_{(m)}$
ACCESS-CM2	-0.199	1.31	0.498
CNRM-CM6-1	0.399	1.053	0.485
FGOALS-f3-L	-1.589	0.722	0.513
FGOALS-g3	-1.713	1.047	0.529
INM-CM4-8	0.63	0.765	0.501
INM-CM5-0	0.074	0.71	0.481
MCM-UA-1-0	-0.229	1.044	0.47
MIROC-ES2L	-0.264	0.774	0.437
UKESM1-0-LL	-0.021	0.636	0.462

Table G: Sea-surface temperature gradients: Calibrated bias-correction coefficients ($\hat{\beta}_0^{(m)}$ and $\hat{\beta}_1^{(m)}$), and standard deviation of noise ($\hat{\sigma}_{(m)}$)

C Detailed calibration results for hazard modules

C.1 Comparison of goodness-of-fit for catastrophe loss distributions

Distributions	AIC	BIC	Rank (AIC)	Rank (BIC)
Log-Normal	9366.825	9366.825	1	1
Weibull	9405.851	9412.683	3	3
Pareto	9379.475	9386.307	2	2
Cauchy	9560.989	9567.821	4	4

Table A: Goodness-of-fit for catastrophe loss distributions: AIC and BIC

C.2 Flood

	Model 1	Model 2	Model 3*	Model 4	Model 5	Model 6
(Intercept)	-2.177**	-4.295**	-3.714**	-4.326**	-3.666**	-4.191**
	(0.004)	(0.002)	(0.001)	(0.005)	(0.002)	(0.002)
Precipitation	0.004**			0.000	0.000	
	(0.005)			(0.967)	(0.902)	
rx1day		0.081**		0.083+		0.041
		(0.002)		(0.098)		(0.515)
rx5day			0.037**		0.035+	0.020
			(0.001)		(0.099)	(0.487)
AIC	138.6	136.1	136.0	138.1	138.0	137.6
BIC	142.7	140.1	140.0	144.1	144.1	143.7
Log.Lik.	-67.306	-66.026	-65.998	-66.025	-65.991	-65.788
F	7.838	9.906	10.511	4.948	5.285	5.269

+ $p < 0.1$, * $p < 0.05$, ** $p < 0.01$, *** $p < 0.001$

Table B: Flood: candidate frequency models

	Model 1	Model 2	Model 3*	Model 4	Model 5	Model 6
Precipitation	0.003+			0.000	-0.001	
	(0.086)			(0.942)	(0.826)	
rx1day		0.071*		0.076		0.004
		(0.049)		(0.335)		(0.963)
rx5day			0.035*		0.040	0.034
			(0.029)		(0.170)	(0.339)
AIC	2000.5	1999.6	1998.7	2001.6	2000.6	2000.6
BIC	2006.1	2005.2	2004.3	2009.1	2008.1	2008.1

+ $p < 0.1$, * $p < 0.05$, ** $p < 0.01$, *** $p < 0.001$

Table C: Flood: candidate severity models

C.3 Bushfire

Here, `mfwixx` represents the annual maximum of the Fire Weather Index averaged across all gridded cells in Australia, while `xfwixx` denotes the highest annual maximum of the Fire Weather Index across all gridded cells. Similarly, `mfwixd` represents the average duration of extreme fire weather across all gridded cells, whereas `xfwixd` denotes the longest duration of extreme fire weather observed across all gridded cells in Australia.

	Model 1*	Model 2	Model 3	Model 4	Model 5	Model 6
mfwixx	0.084**		0.092**			
	(0.002)		(0.001)			
xfwixx		0.004	-0.005			
		(0.418)	(0.482)			
mfwixd				0.072**		0.109**
				(0.001)		(0.007)
xfwixd					0.012	-0.014
					(0.111)	(0.262)
AIC	118.3	127.9	119.7	120.1	126.3	120.8
BIC	122.3	132.0	125.8	124.2	130.3	126.9
Log.Lik.	-57.130	-61.968	-56.858	-58.053	-61.137	-57.394
F	9.889	0.657	5.433	10.195	2.547	5.470

+ $p < 0.1$, * $p < 0.05$, ** $p < 0.01$, *** $p < 0.001$

Table D: Bushfire: candidate frequency models

As all coefficients in the bushfire severity model are statistically insignificant and the stationary Log-Normal distribution yields the lowest AIC and BIC values, we adopt the stationary Log-Normal distribution to model bushfire severity.

	Model 1	Model 2	Model 3	Model 4	Model 5	Model 6
mfwixx	0.016		0.008			
	(0.652)		(0.822)			
xfwixx		0.008	0.007			
		(0.461)	(0.532)			
mfwixd				-0.003		0.029
				(0.931)		(0.603)
xfwixd					-0.004	-0.012
					(0.652)	(0.495)
Num.Obs.	37	37	37	37	37	37
AIC	1527.0	1526.6	1528.6	1527.2	1527.0	1528.7
BIC	1531.8	1531.5	1535.0	1532.0	1531.8	1535.1

+ $p < 0.1$, * $p < 0.05$, ** $p < 0.01$, *** $p < 0.001$

Table E: Bushfire: candidate severity models

C.4 Tropical cyclones

	Model 1*	Model 2	Model 3
Intercept	-33.005***	545.650***	367.462***
	(<0.001)	(<0.001)	(<0.001)
SST	1.213***		0.989***
	(<0.001)		(<0.001)
MSLP		-0.005***	-0.004***
		(<0.001)	(<0.001)
AIC	257.3	258.0	244.1
BIC	266.3	267.0	257.7
Log.Lik.	-126.625	-127.005	-119.067
F	27.719	36.066	16.122

+ $p < 0.1$, * $p < 0.05$, ** $p < 0.01$, *** $p < 0.001$

Table F: Tropical cyclones: candidate frequency models

	Model 1	Model 2	Model 3	Model 4
SST	-79.405			
	(0.189)			
SST^2	1.560			
	(0.194)			
MSLP		-2.022		
		(0.342)		
$MSLP^2$		0.000		
		(0.343)		
cs(SST)			-0.886	-1.096*
			(0.129)	(0.048)
cs(MSLP)				-0.001
				(0.346)
AIC	1612.2	1613.0	1614.5	1613.1
BIC	1618.8	1619.6	1624.3	1629.5

+ p $<$ 0.1, * p $<$ 0.05, ** p $<$ 0.01, *** p $<$ 0.001

Table G: Tropical cyclones: candidate severity models

C.5 Storms

	Model 1*	Model 2	Model 3
Intercept	-11.573***	161.061**	71.386
	($<$0.001)	(0.008)	(0.364)
SST	0.348**		0.260+
	(0.003)		(0.073)
MSLP		-0.002**	-0.001
		(0.007)	(0.291)
AIC	516.1	518.2	517.0
BIC	526.5	528.6	532.6
Log.Lik.	-256.058	-257.101	-255.499
F	8.800	7.240	4.888

+ p $<$ 0.1, * p $<$ 0.05, ** p $<$ 0.01, *** p $<$ 0.001

Table H: Storms: candidate frequency models

	Model 1*	Model 2	Model 3
SST	0.239		0.176
	(0.103)		(0.296)
MSLP		-0.001	-0.001
		(0.149)	(0.471)
AIC	2504.3	2504.9	2505.8
BIC	2510.7	2511.3	2514.3

+ $p < 0.1$, * $p < 0.05$, ** $p < 0.01$, *** $p < 0.001$

Table I: Storms: candidate severity models

C.6 East Coast Low

	Model 1	Model 2*
Intercept	-2.593	-2.260*
	(0.518)	(0.041)
SST	-0.098	
	(0.625)	
SST gradients		2.189+
		(0.053)
AIC	81.7	77.8
BIC	90.7	86.8
Log.Lik.	-38.828	-36.888
F	0.239	3.732

+ $p < 0.1$, * $p < 0.05$, ** $p < 0.01$, *** $p < 0.001$

Table J: East Coast Low: candidate frequency models

Given the limited data and high uncertainty in projected East Coast Low intensities under climate change (Pepler et al., 2016b), we assume a stationary distribution for the normalized severity of East Coast Lows.

C.7 Hailstorms

	Model 1
Intercept	-11.589*
	(0.014)
Atmospheric temperature	-0.079
	(0.452)
Near-surface temperature	0.211***
	(<0.001)
AIC	281.3
BIC	296.9
Log.Lik.	-137.654
F	6.437

+ $p < 0.1$, * $p < 0.05$, ** $p < 0.01$, *** $p < 0.001$

Table K: Hailstorm: frequency model

As all coefficients are statistically insignificant and their signs do not align with expectations (e.g., a positive relationship between near-surface temperature and hailstorm intensity is anticipated), we adopt a stationary Log-Normal distribution to model hailstorm severity.

	Model 1
Atmospheric temperature	-0.049
	(0.724)
Near-surface temperature	-0.083
	(0.394)
AIC	1304.8
BIC	1310.4

+ $p < 0.1$, * $p < 0.05$, ** $p < 0.01$, *** $p < 0.001$

Table L: Hailstorm: severity model

D Comparison of projected damage ratios in literature

The projected economic damage ratios from our climate-dependent DFA model (Section 3.2.2) are compared with estimates from the Dynamic Integrated Model of Climate and the Economy (DICE), originally proposed by Nordhaus (1992). The DICE model has been widely adopted in climate economics to estimate the social cost of carbon and evaluate climate policies. For this comparison, we use damage ratio estimates from the two latest versions of the DICE model: DICE-2023 (Barrage and Nordhaus, 2024) and DICE-2016 (Nordhaus, 2018).

For benchmarking, we focus on three scenarios from the DICE model: baseline, cost-benefit optimal, and 2 °C target. The baseline scenario in DICE assumes a 3.6 °C global temperature increase by 2100 (Barrage and Nordhaus, 2024), which aligns broadly with the SSP 7.0 scenario (4.1 °C by 2100). The cost-benefit optimal scenario projects a 2.6 °C rise by 2100 (Barrage and Nordhaus, 2024), corresponding to SSP 4.5 (2.63 °C by 2100). Lastly, the 2 °C target scenario assumes a 2 °C limit on warming by 2100 (Barrage and Nordhaus, 2024), which is comparable to SSP 2.6 (1.76 °C by 2100) (Riahi et al., 2017). However, caution is warranted, as the narratives underlying the DICE scenarios differ from those of the SSP framework, and here we only focus on temperature alignment. For a detailed discussion of these narratives, see Barrage and Nordhaus (2024).

Figure A presents a comparison between our simulated damage ratios (Section 3.2.2) and the DICE estimates. Since DICE projections are provided at five-year intervals, we apply spline interpolation to convert them to annual values for benchmarking. Our mean projected damage ratios align more closely with DICE-2016 estimates in the early projection horizon but fall below them in later years. Across the entire horizon, our projections are also lower than those from DICE-2023. However, the estimated damage ratios from both DICE-2016 and DICE-2023 generally fall within the 5th–95th percentile prediction intervals of our simulations in the corresponding SSP scenarios, suggesting that our projections encompass their estimated damage paths.

However, caution is warranted when interpreting these benchmarking results. Firstly, the DICE model estimates global climate impacts, whereas our analysis focuses on localised impacts (specifically, Australia). Given the regional heterogeneity in climate risks, economic structures, and infrastructure profiles, differences between the DICE projections and our results are anticipated. Secondly, the DICE model captures the cumulative, long-term economic impacts of global warming using a quadratic damage function (Barrage and Nordhaus, 2024), whereas our simulations focus on the instantaneous impacts of natural catastrophe events, which are more relevant for general insurance applications. We do not account for chronic climate change effects. This distinction may explain the higher damage ratios projected by the DICE model, particularly in the later projection horizon, where cumulative climate impacts on economic outputs become more pronounced.

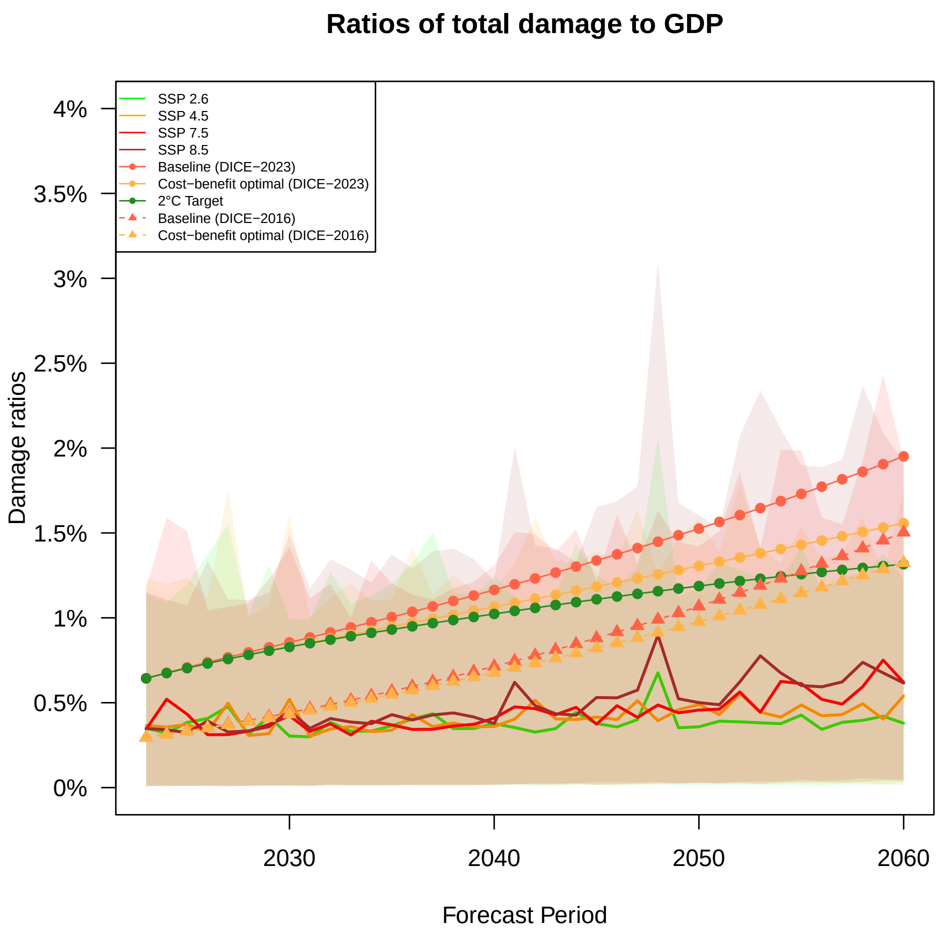

Figure A: Comparison of projected economic damage ratios: Climate-dependent DFA (solid lines), DICE-2023 (circled markers), and DICE-2016 (triangular markers)

References

AASB, 2023. AASB S2: Climate-related Disclosures.

Ahlgrim, K.C., D'Arcy, S.P., Gorvett, R.W., 2005. Modeling financial scenarios: A framework for the actuarial profession, in: Proceedings of the Casualty Actuarial Society, pp. 177–238.

Alien, M., 2003. Liability for climate change: Will it ever be possible to sue anyone for damaging the climate? Nature 421, 891–892.

Allen, J.T., Karoly, D.J., Walsh, K.J., 2014. Future australian severe thunderstorm environments. part ii: The influence of a strongly warming climate on convective environments. Journal of Climate 27, 3848–3868.

APRA, 2023. Gps 114: Capital adequacy – asset risk charge. URL: https://www.apra.gov.au/gps-114-capital-adequacy-asset-risk-charge. accessed: 2025-05-06.

APRA, 2024a. Annual general insurance institution-level statistics. https://www.apra.gov.au/annual-general-insurance-institution-level-statistics. Accessed: 2024-06-30.

APRA, 2024b. Quarterly general insurance performance statistics. URL: https://www.apra.gov.au/quarterly-general-insurance-performance-statistics. regularly updated dataset on general insurance performance metrics.

APRA, 2024c. Quarterly general insurance performance statistics. https://www.apra.gov.au/quarterly-general-insurance-performance-statistics. Accessed: 2024-06-30.

Australian Bureau of Statistics, 2024a. Business Indicators, Australia. https://www.abs.gov.au/statistics/economy/business-indicators/business-indicators-australia/latest-release. Accessed: 2024-06-30.

Australian Bureau of Statistics, 2024b. Consumer Price Index, Australia. https://www.abs.gov.au/statistics/economy/price-indexes-and-inflation/consumer-price-index-australia/latest-release. Accessed: 2024-06-30.

Australian Prudential Regulation Authority, 2023. Insurance climate vulnerability assessment. URL: https://www.apra.gov.au/insurance-climate-vulnerability-assessment. accessed: 2025-05-06.

Bansal, R., Kiku, D., Ochoa, M., 2019. Climate change risk. Federal Reserve Bank of San Francisco Working Paper .

Barnett, M., 2023. Climate change and uncertainty: An asset pricing perspective. Management Science .

Barrage, L., Nordhaus, W., 2024. Policies, projections, and the social cost of carbon: Results from the dice-2023 model. Proceedings of the National Academy of Sciences 121, e2312030121.

Bégin, J.F., 2022. Ensemble economic scenario generators: Unity makes strength. North American Actuarial Journal , 1–28.

Bertram, C., Hilaire, J., Kriegler, E., Beck, T., Bresch, D.N., Clarke, L., Cui, R., Edmonds, J., Min, J., Piontek, F., et al., 2020. Ngfs climate scenarios database: Technical documentation.

Bloemendaal, N., Haigh, I.D., de Moel, H., Muis, S., Haarsma, R.J., Aerts, J.C., 2020. Generation of a global synthetic tropical cyclone hazard dataset using storm. Scientific data 7, 40.

Bower, E., Weerasinghe, S., 2021. Leaving place, restoring home: enhancing the evidence base on planned relocation cases in the context of hazards, disasters, and climate change. UNSW Sydney and Kaldor Centre for International Refugee Law .

Boyer, M.M., Jacquier, E., Van Norden, S., 2012. Are underwriting cycles real and forecastable? Journal of Risk and Insurance 79, 995–1015.

Bullock, D., 2022. Public nuisance and climate change: The common law's solutions to the plaintiff, defendant and causation problems. The Modern Law Review 85, 1136–1167.

Bureau of Meteorology, . The southern oscillation index (soi). http://www.bom.gov.au/climate/enso/history/ln-2010-12/SOI-what.shtml. Accessed: 2023-10-09.

Bylund, E., Jonsson, M., 2020. How does climate change affect the long-run real interest rate. Economic Commentaries 11, 90–108.

Cevik, S., Jalles, J.T., 2022. This changes everything: Climate shocks and sovereign bonds□. Energy Economics 107, 105856.

Chen, H., Cummins, J.D., Sun, T., Weiss, M.A., 2020. The reinsurance network among us property–casualty insurers: Microstructure, insolvency risk, and contagion. Journal of Risk and Insurance 87, 253–284.

Chen, W., Koo, B., Wang, Y., O'Hare, C., Langrené, N., Toscas, P., Zhu, Z., 2021. Using a stochastic economic scenario generator to analyse uncertain superannuation and retirement outcomes. Annals of Actuarial Science 15, 549–566.

Christiansen, M.C., Niemeyer, A., 2014. Fundamental definition of the solvency capital requirement in solvency ii. ASTIN Bulletin: The Journal of the IAA 44, 501–533.

Ciccarelli, M., Kuik, F., Hernández, C.M., 2023. The asymmetric effects of weather shocks on euro area inflation.

Consigli, G., Moriggia, V., Vitali, S., Mercuri, L., 2018. Optimal insurance portfolios risk-adjusted performance through dynamic stochastic programming. Computational Management Science 15, 599–632.

Copernicus Climate Change Service, 2024a. CMIP6 climate projections. https://cds.climate.copernicus.eu/cdsapp#!/dataset/projections-cmip6?tab=overview. Accessed: 2024-06-30.

Copernicus Climate Change Service, 2024b. ERA5-Land monthly averaged data from 1950 to present. https://cds.climate.copernicus.eu/cdsapp#!/dataset/reanalysis-era5-land-monthly-means?tab=overview. Accessed: 2024-06-30.

Copernicus Climate Change Service, 2024c. Historical Normalised Catastrophe list - December 2024. https://insurancecouncil.com.au/wp-content/uploads/2025/01/ICA-Historical-Normalised-Catastrophe-Master-December-2024.xlsx. Accessed: 2024-06-30.

Coutts, S.M., Devitt, R., 1989. The assessment of the financial strength of insurance companies by a generalized cash flow model, in: Financial models of insurance solvency. Springer, pp. 1–36.

Crompton, R.P., McAneney, K.J., 2008. Normalised australian insured losses from meteorological hazards: 1967–2006. Environmental Science & Policy 11, 371–378.

Cummins, J.D., Outreville, J.F., 1985. An international analysis of underwriting cycles in property-liability insurance. Foundations of Insurance Economics: Readings in Economics and Finance , 609–625.

D'Arcy, S.P., Gorvett, R.W., 2004. The use of dynamic financial analysis to determine whether an optimal growth rate exists for a property-liability insurer. Journal of Risk and Insurance 71, 583–615.

Dellink, R., Chateau, J., Lanzi, E., Magné, B., 2017a. Long-term economic growth projections in the shared socioeco-

nomic pathways. Global Environmental Change 42, 200–214.
Dellink, R., Chateau, J., Lanzi, E., Magné, B., 2017b. Long-term economic growth projections in the shared socioeconomic pathways. Global Environmental Change 42, 200–214.
Dicks, D.L., Garven, J.R., 2022. Asymmetric information and insurance cycles. Journal of Risk and Insurance 89, 449–474.
Dowdy, A.J., 2018. Climatological variability of fire weather in australia. Journal of Applied Meteorology and Climatology 57, 221–234.
Economides, G., Xepapadeas, A., 2018. Monetary policy under climate change .
Eisenberg, D., 2004. The mixed effects of precipitation on traffic crashes. Accident analysis & prevention 36, 637–647.
Eling, M., Parnitzke, T., 2007. Dynamic financial analysis: Classification, conception, and implementation. Risk Management and Insurance Review 10, 33–50.
Eling, M., Parnitzke, T., Schmeiser, H., 2008. Management strategies and dynamic financial analysis. Variance 2, 52–70.
Eling, M., Toplek, D., 2009. Modeling and management of nonlinear dependencies–copulas in dynamic financial analysis. Journal of Risk and Insurance 76, 651–681.
EM–DAT, 2023. The international disasters database. Data retrieved from `https://public.emdat.be/data`.
Erdogan, K., 2013. Spline interpolation techniques. Journal of Technical Science and Technologies , 47–52.
Eyring, V., Bony, S., Meehl, G.A., Senior, C.A., Stevens, B., Stouffer, R.J., Taylor, K.E., 2016. Overview of the coupled model intercomparison project phase 6 (cmip6) experimental design and organization. Geoscientific Model Development 9, 1937–1958.
Faccia, D., Parker, M., Stracca, L., 2021. Feeling the heat: extreme temperatures and price stability.
FactSet, 2024. FactSet Database. Available at: `https://www.factset.com/`. Accessed on 2024-06-30.
Gatzert, N., Özdil, O., 2024. The impact of dependencies between climate risks on the asset and liability side of non-life insurers. European Actuarial Journal , 1–19.
Görgen, M., Jacob, A., Nerlinger, M., Riordan, R., Rohleder, M., Wilkens, M., 2020. Carbon risk. Available at SSRN 2930897 .
Grimm, W.M., 2023. On volatile growth: Simple fitting of exponential functions taking into account values of every observation with any signs, applied to readily calculate a novel covariance-invariant cagr. The Engineering Economist 68, 34–58.
Grippa, P., Mann, S., 2020. Climate-related stress testing: Transition risks in norway. IMF Working Papers 2020.
Haug, O., Dimakos, X.K., Vårdal, J.F., Aldrin, M., Meze-Hausken, E., 2011. Future building water loss projections posed by climate change. Scandinavian Actuarial Journal 2011, 1–20.
Heal, G., Park, J., 2016. Reflections—temperature stress and the direct impact of climate change: a review of an emerging literature. Review of Environmental Economics and Policy .
Holston, K., Laubach, T., Williams, J.C., 2017. Measuring the natural rate of interest: International trends and determinants. Journal of International Economics 108, S59–S75.
Hong, H., Li, F.W., Xu, J., 2019. Climate risks and market efficiency. Journal of econometrics 208, 265–281.
IFRS, 2023. Ifrs s2: Sustainability disclosure standard. `https://www.ifrs.org/issued-standards/ifrs-sustainability-standards-navigator/ifrs-s2-climate-related-disclosures/#standard`.
IPCC, 2021a. Climate change 2021: The physical science basis. contribution of working group i to the sixth assessment report of the ipcc – chapter 11. Cambridge University Press. URL: `https://www.ipcc.ch/report/ar6/wg1/`.
IPCC, 2021b. Climate change 2021: The physical science basis. contribution of working group i to the sixth assessment report of the ipcc – chapter 12. Cambridge University Press. URL: `https://www.ipcc.ch/report/ar6/wg1/`.
Jagger, T.H., Elsner, J.B., Burch, R.K., 2011. Climate and solar signals in property damage losses from hurricanes affecting the united states. Natural Hazards 58, 541–557.
Jagger, T.H., Elsner, J.B., Saunders, M.A., 2008. Forecasting us insured hurricane losses. Climate extremes and society 189, 209.
Jain, S., Scaife, A.A., Shepherd, T.G., Deser, C., Dunstone, N., Schmidt, G.A., Trenberth, K.E., Turkington, T., 2023. Importance of internal variability for climate model assessment. npj Climate and Atmospheric Science 6, 68.
James, G., Witten, D., Hastie, T., Tibshirani, R., et al., 2013. An introduction to statistical learning. volume 112. Springer.
Jarzabkowski, P., Meissner, K., Unger, C., 2022. Australia's new cyclone reinsurance pool: Implications for insurance in a climate changed future. Australian Environment Review 37, 43–45.
Jørgensen, B., Paes De Souza, M.C., 1994. Fitting tweedie's compound poisson model to insurance claims data. Scandinavian Actuarial Journal 1994, 69–93.
Karydas, C., Xepapadeas, A., 2022. Climate change financial risks: Implications for asset pricing and interest rates. Journal of Financial Stability 63, 101061.

Kaufmann, R., Gadmer, A., Klett, R., 2001. Introduction to dynamic financial analysis. ASTIN Bulletin: The Journal of the IAA 31, 213–249.

Keen, S., Lenton, T.M., Godin, A., Yilmaz, D., Grasselli, M., Garrett, T.J., 2021. Economists' erroneous estimates of damages from climate change. arXiv preprint arXiv:2108.07847 .

Kilic Celik, S., Kose, A.M., Ohnsorge, F., Ruch, F., 2023. Potential growth: A global database.

Klugman, S.A., Panjer, H.H., Willmot, G.E., 2012. Loss models: from data to decisions. volume 715. John Wiley & Sons.

Klusak, P., Agarwala, M., Burke, M., Kraemer, M., Mohaddes, K., 2023. Rising temperatures, falling ratings: The effect of climate change on sovereign creditworthiness. Management Science 69, 7468–7491.

Kodra, E., Bhatia, U., Chatterjee, S., Chen, S., Ganguly, A.R., 2020. Physics-guided probabilistic modeling of extreme precipitation under climate change. Scientific reports 10, 10299.

Kotz, M., Kuik, F., Lis, E., Nickel, C., 2024. Global warming and heat extremes to enhance inflationary pressures. Nature Communications Earth & Environment 5, 1–13.

Kunreuther, H., Michel-Kerjan, E., Ranger, N., 2011. Insuring climate catastrophes in Florida: an analysis of insurance pricing and capacity under various scenarios of climate change and adaptation measures. Technical Report. Grantham Research Institute on Climate Change and the Environment.

Kunreuther, H.C., Michel-Kerjan, E.O., 2011. At war with the weather: Managing large-scale risks in a new era of catastrophes. MIT Press.

Laubach, T., Williams, J.C., 2003. Measuring the natural rate of interest. Review of Economics and Statistics 85, 1063–1070.

Lenton, T.M., Held, H., Kriegler, E., Hall, J.W., Lucht, W., Rahmstorf, S., Schellnhuber, H.J., 2008. Tipping elements in the earth's climate system. Proceedings of the national Academy of Sciences 105, 1786–1793.

Leslie, L.M., Leplastrier, M., Buckley, B.W., 2008. Estimating future trends in severe hailstorms over the sydney basin: A climate modelling study. Atmospheric Research 87, 37–51.

Lettau, M., Ludvigson, S.C., 2005. Expected returns and expected dividend growth. Journal of Financial Economics 76, 583–626.

Liu, P.R., Raftery, A.E., 2021. Country-based rate of emissions reductions should increase by 80% beyond nationally determined contributions to meet the 2 degree target. Communications earth & environment 2, 29.

Lyubchich, V., Kilbourne, K.H., Gel, Y.R., Richardson, T., 2017. Where home insurance meets climate change: Making sense of climate risk, data uncertainty, and projections. Variance 12, 278–292.

Lyubchich, V., Newlands, N.K., Ghahari, A., Mahdi, T., Gel, Y.R., 2019. Insurance risk assessment in the face of climate change: Integrating data science and statistics. Wiley Interdisciplinary Reviews: Computational Statistics 11, e1462.

Mallucci, E., 2022. Natural disasters, climate change, and sovereign risk. Journal of International Economics 139, 103672.

Maraun, D., 2013. Bias correction, quantile mapping, and downscaling: Revisiting the inflation issue. Journal of Climate 26, 2137–2143.

McGuire, G., 2008. Does rainfall increase or decrease motor accidents? .

McNeil, A.J., Frey, R., Embrechts, P., 2015. Quantitative risk management: concepts, techniques and tools-revised edition. Princeton university press.

Meier, U.B., Outreville, J.F., 2006. Business cycles in insurance and reinsurance: the case of france, germany and switzerland. The Journal of Risk Finance .

Meier, U.B., Outreville, J.F., 2010. Business cycles in insurance and reinsurance: international diversification effects. Applied Financial Economics 20, 659–668.

Meiler, S., Vogt, T., Bloemendaal, N., Ciullo, A., Lee, C.Y., Camargo, S.J., Emanuel, K., Bresch, D.N., 2022. Intercomparison of regional loss estimates from global synthetic tropical cyclone models. Nature Communications 13, 6156.

Mitchell-Wallace, K., Jones, M., Hillier, J., Foote, M., 2017. Natural catastrophe risk management and modelling: A practitioner's guide. John Wiley & Sons.

Mongelli, F.P., Pointner, W., van den End, J.W., 2022. The effects of climate change on the natural rate of interest: a critical survey .

Mora, C., Dousset, B., Caldwell, I.R., Powell, F.E., Geronimo, R.C., Bielecki, C.R., Counsell, C.W., Dietrich, B.S., Johnston, E.T., Louis, L.V., et al., 2017. Global risk of deadly heat. Nature climate change 7, 501–506.

Mukherjee, K., Ouattara, B., 2021. Climate and monetary policy: do temperature shocks lead to inflationary pressures? Climatic change 167, 32.

Neal, T., Newell, B.R., Pitman, A.J., 2025. Reconsidering the macroeconomic damage of severe warming. Environmental Research Letters .

Nordhaus, W., 2013. The climate casino: Risk, uncertainty, and economics for a warming world. Yale University Press.

Nordhaus, W., 2018. Evolution of modeling of the economics of global warming: changes in the dice model, 1992–2017. Climatic change 148, 623–640.

Nordhaus, W.D., 1992. The dice model: background and structure of a dynamic integrated climate-economy model of the economics of global warming .

O Neill, B.C., Kriegler, E., Ebi, K.L., Kemp-Benedict, E., Riahi, K., Rothman, D.S., Van Ruijven, B.J., Van Vuuren, D.P., Birkmann, J., Kok, K., et al., 2017. The roads ahead: Narratives for shared socioeconomic pathways describing world futures in the 21st century. Global environmental change 42, 169–180.

OECD, 2023. Global insurance market trends 2023. OECD Publishing URL: https://www.oecd.org/finance/insurance/global-insurance-market-trends.htm.

Parker, M., 2018. The impact of disasters on inflation. Economics of Disasters and Climate Change 2, 21–48.

Paudel, Y., Botzen, W., Aerts, J., 2013. Estimation of insurance premiums for coverage against natural disaster risk: an application of bayesian inference. Natural Hazards and Earth System Sciences 13, 737–754.

Paudel, Y., Botzen, W., Aerts, J., Dijkstra, T., 2015. Risk allocation in a public–private catastrophe insurance system: an actuarial analysis of deductibles, stop-loss, and premiums. Journal of Flood Risk Management 8, 116–134.

Paulson, A.S., Dixit, R., 1989. Cash flow simulation models for premium and surplus analysis, in: Financial Models of Insurance Solvency. Springer, pp. 37–55.

Pepler, A.S., Alexander, L.V., Evans, J.P., Sherwood, S.C., 2016a. The influence of local sea surface temperatures on australian east coast cyclones. Journal of Geophysical Research: Atmospheres 121, 13–352.

Pepler, A.S., Di Luca, A., Ji, F., Alexander, L.V., Evans, J.P., Sherwood, S.C., 2016b. Projected changes in east australian midlatitude cyclones during the 21st century. Geophysical Research Letters 43, 334–340.

Pielke, R., 2021. Economic ‘normalisation’of disaster losses 1998–2020: A literature review and assessment. Environmental Hazards 20, 93–111.

Pielke, R.A., Landsea, C.W., 1998. Normalized hurricane damages in the united states: 1925–95. Weather and forecasting 13, 621–631.

Quilcaille, Y., Batibeniz, F., Ribeiro, A.F., Padrón, R.S., Seneviratne, S.I., 2022. Fire weather index data under historical and ssp projections in cmip6 from 1850 to 2100. Earth System Science Data Discussions 2022, 1–31.

Ramsey, F.P., 1928. A mathematical theory of saving. The economic journal 38, 543–559.

Raupach, T.H., Martius, O., Allen, J.T., Kunz, M., Lasher-Trapp, S., Mohr, S., Rasmussen, K.L., Trapp, R.J., Zhang, Q., 2021. The effects of climate change on hailstorms. Nature reviews earth & environment 2, 213–226.

Reig Torra, J., Guillen, M., Pérez-Marín, A.M., Rey Gámez, L., Aguer, G., 2023. Weather conditions and telematics panel data in monthly motor insurance claim frequency models. Risks 11, 57.

Reserve Bank of Australia, 2024. Cash Rate Target. https://www.rba.gov.au/statistics/cash-rate/. Accessed: 2024-06-30.

Riahi, K., Van Vuuren, D.P., Kriegler, E., Edmonds, J., O’neill, B.C., Fujimori, S., Bauer, N., Calvin, K., Dellink, R., Fricko, O., et al., 2017. The shared socioeconomic pathways and their energy, land use, and greenhouse gas emissions implications: An overview. Global environmental change 42, 153–168.

Sanabria, L.A., Qin, X., Li, J., Cechet, R.P., 2022. Bias correction of extreme values of high-resolution climate simulations for risk analysis. Theoretical and Applied Climatology 150, 1015–1026.

Scheel, I., Ferkingstad, E., Frigessi, A., Haug, O., Hinnerichsen, M., Meze-Hausken, E., 2013. A bayesian hierarchical model with spatial variable selection: the effect of weather on insurance claims. Journal of the Royal Statistical Society Series C: Applied Statistics 62, 85–100.

Seneviratne, S.I., Zhang, X., Adnan, M., Badi, W., Dereczynski, C., Di Luca, A., Ghosh, S., Iskander, I., Kossin, J., Lewis, S., et al., 2021. Weather and climate extreme events in a changing climate (chapter 11) .

Sharples, J.J., Cary, G.J., Fox-Hughes, P., Mooney, S., Evans, J.P., Fletcher, M.S., Fromm, M., Grierson, P.F., McRae, R., Baker, P., 2016. Natural hazards in australia: extreme bushfire. Climatic Change 139, 85–99.

Speer, M., Leslie, L., Hartigan, J., MacNamara, S., 2021. Changes in frequency and location of east coast low pressure systems affecting southeast australia. Climate 9, 44.

Taylor, G., 2008. A simple model of insurance market dynamics. North American Actuarial Journal 12, 242–262.

Tesselaar, M., Botzen, W.W., Aerts, J.C., 2020. Impacts of climate change and remote natural catastrophes on eu flood insurance markets: An analysis of soft and hard reinsurance markets for flood coverage. Atmosphere 11, 146.

Trading Economics, 2024. Australia Corporate Tax Rate. https://tradingeconomics.com/australia/corporate-tax-rate. Accessed: 2024-06-30.

Venturini, A., 2022. Climate change, risk factors and stock returns: A review of the literature. International Review of Financial Analysis 79, 101934.

Vranes, K., Pielke Jr, R., 2009. Normalized earthquake damage and fatalities in the united states: 1900–2005. Natural

Hazards Review 10, 84–101.
Weinkle, J., Pielke Jr, R., 2017. The truthiness about hurricane catastrophe models. Science, Technology, & Human Values 42, 547–576.
Wilkie, A.D., 1995. More on a stochastic asset model for actuarial use. British Actuarial Journal 1, 777–964.
Winter, R.A., 1988. The liability crisis and the dynamics of competitive insurance markets. Yale J. on Reg. 5, 455.
Winter, R.A., 1994. The dynamics of competitive insurance markets. Journal of Financial Intermediation 3, 379–415.
World Bank Group, 2024. Databank: World Development Indicators. `https://databank.worldbank.org/source/world-development-indicators`. Accessed: 2024-06-30.
Wu, Y., Miao, C., Fan, X., Gou, J., Zhang, Q., Zheng, H., 2022. Quantifying the uncertainty sources of future climate projections and narrowing uncertainties with bias correction techniques. Earth's Future 10, e2022EF002963.
Yazici, B., Yolacan, S., 2007. A comparison of various tests of normality. Journal of statistical computation and simulation 77, 175–183.